

Report on FY15 Alloy 617 SMT Creep-Fatigue Test Results



Approved for public release;
distribution is unlimited.

Yanli Wang
Robert I. Jetter
Seth T. Baird
Chao Pu
T.-L. Sham

June 22, 2015

DOCUMENT AVAILABILITY

Reports produced after January 1, 1996, are generally available free via US Department of Energy (DOE) SciTech Connect.

Website <http://www.osti.gov/scitech/>

Reports produced before January 1, 1996, may be purchased by members of the public from the following source:

National Technical Information Service
5285 Port Royal Road
Springfield, VA 22161
Telephone 703-605-6000 (1-800-553-6847)
TDD 703-487-4639
Fax 703-605-6900
E-mail info@ntis.gov
Website <http://www.ntis.gov/help/ordermethods.aspx>

Reports are available to DOE employees, DOE contractors, Energy Technology Data Exchange representatives, and International Nuclear Information System representatives from the following source:

Office of Scientific and Technical Information
PO Box 62
Oak Ridge, TN 37831
Telephone 865-576-8401
Fax 865-576-5728
E-mail reports@osti.gov
Website <http://www.osti.gov/contact.html>

This report was prepared as an account of work sponsored by an agency of the United States Government. Neither the United States Government nor any agency thereof, nor any of their employees, makes any warranty, express or implied, or assumes any legal liability or responsibility for the accuracy, completeness, or usefulness of any information, apparatus, product, or process disclosed, or represents that its use would not infringe privately owned rights. Reference herein to any specific commercial product, process, or service by trade name, trademark, manufacturer, or otherwise, does not necessarily constitute or imply its endorsement, recommendation, or favoring by the United States Government or any agency thereof. The views and opinions of authors expressed herein do not necessarily state or reflect those of the United States Government or any agency thereof.

Materials Science and Technology Division

Report on FY15 Alloy 617 SMT Creep-Fatigue Test Results

Yanli Wang, Robert I. Jetter*, Seth T. Baird, Chao Pu**, T.-L. Sham

* Consultant

** University of Tennessee, Knoxville

Date Published: June 22, 2015

Prepared by
OAK RIDGE NATIONAL LABORATORY
Oak Ridge, Tennessee 37831-6283
managed by
UT-BATTELLE, LLC
for the
US DEPARTMENT OF ENERGY
under contract DE-AC05-00OR22725

Page Intentionally Blank

CONTENTS

	Page
LIST OF FIGURES	v
LIST OF TABLES	vii
ACRONYMS	ix
ACKNOWLEDGMENTS	xi
ABSTRACT.....	1
1. INTRODUCTION	3
2. SMT METHODOLOGY	5
2.1 Elastic Follow-up	5
2.2 Conceptual Basis of SMT Approach	5
2.3 SMT Specimen Characteristics	6
2.4 YSMT DEVELOPMENT AND VERIFICATION	7
3. TEST DESCRIPTION.....	9
3.1 Materials	9
3.1.1 Alloy 617	9
3.1.2 Stainless steel 316H	11
3.2 Specimen Sizing.....	11
3.2.1 SMT specimen design.....	12
3.2.2 YSMT Specimen Design	14
3.3 Experimental Setup.....	16
3.3.1 SMT Testing and Instrumentation	16
3.3.2 YSMT Testing System.....	18
4. TEST RESULTS	20
4.1 SMT Creep-fatigue of Alloy 617	20
4.2 SMT Creep-Fatigue of SS316H.....	23
4.3 SMT Creep-Fatigue Testing of SS304H.....	25
4.4 YSMT Creep-Fatigue Testing of SS316H.....	28
5. Creep-Fatigue Code Case Verification	30
5.1 Test Article Geometry and Test Setup.....	30
5.2 Alloy 617 Shakedown Evaluation.....	31
5.2.1 Alloy 617 Material Parameters	31
5.2.2 Alloy 617 Test Conditions Evaluation.....	32
5.3 SS316H Shakedown Evaluation	35
5.4 Comparison based on allowable design life.....	36
6. SUMMARY.....	38
7. REFERENCES	40

Page Intentionally Blank

LIST OF FIGURES

Figure	Page
Fig. 1. Definition of elastic follow-up.....	5
Fig. 2. SMT methodology.....	6
Fig. 3. YSMT test concept.....	8
Fig. 4. Schematic of the layout of the specimens on the Alloy 617 plate.....	10
Fig. 5. Optical images of the as-received Alloy 617 plate for the cross-sectional plane normal to the rolling direction.....	10
Fig. 6. Optical images of the as-received SS316H.....	11
Fig. 7. Type 1 SMT solid bar specimen design.....	13
Fig. 8. (a) YSMT, (b) tubular YSMT and (c) SMT configuration and corresponding FEA model.....	14
Fig. 9. Buckling contour plot for (a) YSMT, (b) tubular YSMT and (c) SMT models.....	15
Fig. 10. YSMT test specimen configuration.....	16
Fig. 11. Applied end-displacement profile for one cycle of creep-fatigue testing.....	16
Fig. 12. SMT test system.....	17
Fig. 13. The YSMT system.....	18
Fig. 14. Test results for test #17 (Alloy 617-950 °C).....	21
Fig. 15. Test results for test #18 (Alloy 617-950 °C).....	21
Fig. 16. Test results for test #21 (Alloy 617-850 °C).....	22
Fig. 17. Test results for test #22 (Alloy 617-850 °C).....	22
Fig. 18. Picture of SS316H after testing (from previous testing).....	24
Fig. 19. Test results for test #19 (SS316H-815 °C).....	24
Fig. 20. Test results for test #20 (SS316H-650 °C).....	25
Fig. 21. Test results for test #24 (SS304H-815 °C).....	26
Fig. 22. Test results for test #25 (SS304H-815 °C).....	27
Fig. 23. Test results for test #26 (SS304H-650 °C).....	27
Fig. 24. Picture of YSMT specimen after testing.....	28
Fig. 25. Test results for YSMT tubular specimen(SS316-815 °C).....	29
Fig. 26. Drawings for the Two SMT Test Articles (Dimensions in Inches).....	30
Fig. 27. Test setup of the SMT specimen.....	31
Fig. 28. Profiles of ΔL for imposing the prescribed displacements over the gage length L for Alloy 617. Displacement hold was applied at the maximum tensile ΔL value. Cycles were fully reversed.....	33
Fig. 29. Typical axisymmetric finite element meshes for Type I and Type II SMT test articles.....	34
Fig. 30. Profile of ΔL for imposing the prescribed displacements over the gage length L for 316H.....	36
Fig. 31. Creep-fatigue code case allowable life comparison to Alloy 617 SMT data.....	37
Fig. 32. Creep-fatigue code case allowable life comparison to SS316H SMT data.....	38

Page Intentionally Blank

LIST OF TABLES

Table	Page
Table 1. Chemical compositions of Alloy 617 plate with heat number 314626 (weight %)	9
Table 2. Chemical compositions of SS304H bar with heat number E131181 (weight %)	10
Table 3. Chemical compositions of SS316H bar with heat number 101076 (weight %)	11
Table 4. SMT testing specimen geometry	13
Table 5. Buckling load and stress values for each model	15
Table 6. YSMT parameters.....	19
Table 7. SMT creep-fatigue for Alloy 617	20
Table 8. SMT creep-fatigue for SS316H	23
Table 9. SMT creep-fatigue for SS304H	25
Table 10. YSMT parameters.....	28
Table 11. SMT test conditions and data for Alloy 617	32
Table 12. Material parameters used in the E-PP finite element analyses for Alloy 617.....	35
Table 13. SMT test conditions and data for 316H SS.....	35
Table 14. Material parameters used in the E-PP finite element analysis for 316H.....	36
Table 15. Experimental Data – Alloy 617 at 950°C.....	37
Table 16. Experimental Data – SS316H at 815°C	38

Page Intentionally Blank

ACRONYMS

ASME	American Society of Mechanical Engineers
ANL	Argonne National Laboratory
SCF	Stress Concentration Factor
DOE	Department of Energy
E-PP	Elastic-Perfectly Plastic
FEA	Finite Element Analysis
HTGR	High Temperature Gas-cooled Reactor
IHX	Intermediate Heat Exchanger
INL	Idaho National Laboratory
LWR	Light Water Reactor
NGNP	Next Generation Nuclear Plant
ORNL	Oak Ridge National Laboratory
SMR	Small Module Reactor
SMT	Simplified Module Test
VHTR	Very High Temperature Reactor

Page Intentionally Blank

ACKNOWLEDGMENTS

This research was sponsored by the U.S. Department of Energy (DOE), Office of Nuclear Energy (NE), for the Advanced Reactor Technologies (ART) Program. We gratefully acknowledge the support provided by Carl Sink of DOE-NE, Advanced Reactor Technologies, ART Program Manager; William Corwin of DOE-NE, ART Materials Technology Lead; David Petti of Idaho National Laboratory (INL), ART Co-National Technical Director; and Richard Wright of INL, Technical Lead, High Temperature Materials.

Helpful discussion with Peter Carter of Stress Engineering Services, Inc. is gratefully acknowledged. Donald Erdman of Oak Ridge National Laboratory (ORNL) programmed the controls. The optical microscopic images of SS316H were provided by Yukinori Yamamoto of ORNL. Technical support from Jeremy Moser, David Thomas and Shane Hawkins of ORNL is greatly appreciated. The time spent by Hong Wang of ORNL in reviewing this report is greatly appreciated.

We would also like to acknowledge Richard Wright for supplying the Alloy 617 materials to support the testing task of this work.

Page Intentionally Blank

ABSTRACT

For the temperature range of $900^{\circ}\text{C} - 950^{\circ}\text{C}$, Alloy 617 is a candidate IHX structural material for high temperature gas reactors (HTGRs) because of its high temperature creep properties. Also, its superior strength over a broad temperature range also offers advantages for certain component applications. In order for the designers to be able to use Alloy 617 for these high temperature components, Alloy 617 has to be approved for use in Section III (the nuclear section) of the ASME (American Society of Mechanical Engineers) Boiler and Pressure Vessel Code. A plan has been developed to propose a Code Case for use of Alloy 617 at elevated temperature in Section III of the ASME Code by September 2015.

There has not been a new high temperature material approved for use in Section III for almost 20 years. The Alloy 617 Code Case effort would lead the way to establish a path for Code qualification of new high temperature materials of interest to other advanced SMRs.

Creep-fatigue at elevated temperatures is the most damaging structural failure mode. In the past 40 years significant efforts have been devoted to the elevated temperature Code rule development in Section III, Subsection NH* of the ASME Boiler and Pressure Vessel Code, to ascertain conservative structural designs to prevent creep-fatigue failure.

The current Subsection NH creep-fatigue procedure was established by the steps of (1) analytically obtaining a detailed stress-strain history, (2) comparing the stress and strain components to cyclic test results deconstructed into stress and strain quantities, and (3) recombining the results to obtain a damage function in the form of the so-called creep-fatigue damage-diagram. The deconstruction and recombination present difficulties in evaluation of test data and determination of cyclic damage in design. The uncertainties in these steps lead to the use of overly conservative design factors in the current creep-fatigue procedure. In addition, and of major significance to the viability of the Alloy 617 Code Case, the use of the current elastic analysis based rules in Subsection NH for the evaluation of strain limits (a precursor for the creep-fatigue rules) and the creep-fatigue rules themselves have been deemed inappropriate for Alloy 617 at temperatures above 650°C (1200°F) (Corum and Brass, 1991). The rationale for this exclusion is that at higher temperatures it is not feasible to decouple plasticity and creep, which is the basis for the current simplified rules. This temperature, 650°C (1200°F), is well below the temperature range of interest for this material for the High Temperature Gas Cooled Reactor (HTGR) as well as the VHTR. The only current alternative is, thus, a full inelastic analysis which requires sophisticated material models which have not yet been formulated and verified.

To address the prohibition on the use of current methods at very high temperatures, proposed Code rules have been developed which are based on the use of elastic-perfectly plastic (E-PP) analysis methods and which are expected to be applicable to very high temperatures. To provide data to implement the proposed rules and to verify their application, a series of tests have been initiated. One test concept, the Simplified Model Test (SMT), takes into account the stress and strain redistribution in real structures by including representative follow-up characteristics in the test specimen. The correlation parameter between test and design is the elastically calculated strain, and the dependent test variable is the observed cycles to failure. Although the initial priority for the SMT approach is to generate data to support validation of the E-PP Code Case for evaluation of creep-fatigue damage, the broader goal of the SMT approach is to develop a methodology for evaluation of creep fatigue damage which is simpler to implement than the current complex rules and applicable to the full temperature range from ambient conditions to the very high temperature creep regime of 900°C to 950°C . Also, guidance has been received from ASME Code committees that the proposed EPP methodology for evaluation of creep-fatigue damage should be extended to the other Subsection NH materials to the extent feasible. Thus, the scope of testing has been expanded to include SS304H and SS316H.

This report describes the SMT approach and the development of testing capability to conduct SMT experiments on Alloy 617 and 304H and 316H and stainless steels. These SMT specimen data are also representative of component loading conditions and have been used as part of the verification of the

proposed elastic-perfectly plastic Code Cases. Results from the SMT tests on both Alloy 617 and SS316H were compared to the predictions from the EPP Creep-Fatigue Code Case. Two different comparisons were made; one based on design life equal to the test duration and the other with an acceptable design life determined from the EPP Code Case procedure. The latter approach permits the determination of a quantitative margin while the former is a “go-no go” comparison. In all cases it is evident that there is a significant design margin between the Creep-fatigue Code Case allowable life and the experimentally measured life for both Alloy 617 and 316H stainless steel.

* Effective July, 2015 with the release of the 2015 Edition of the ASME B&PV Code, Subsection NH is being transferred to Section III, Div. 5, Subsection HBB. However, since this report will be released before Subsection HBB is generally available, reference to Subsection NH will be maintained.

1. INTRODUCTION

This is the FY 15 milestone report on the use of test specimens specifically designed to represent key features of representative components in the development and verification of high temperature design criteria. The following discussion is an abridged version of prior introductory remarks followed by an overview of the activities of the current reporting period.

Due to its strength at very high temperatures up to 950°C , Alloy 617 is the reference material for Very High Temperature Reactor (VHTR) components that operate at or near the outlet gas temperature of the reactor. However, the current rules in Subsection NH for the evaluation of strain limits and creep-fatigue damage using simplified methods based on elastic analysis have been deemed inappropriate for Alloy 617 at temperatures above 650°C (1200°F) (Corum and Brass, 1991). The rationale for this exclusion is that at higher temperatures it is not feasible to decouple plasticity and creep, which is the basis for the current simplified rules. This temperature, 650°C (1200°F), is well below the temperature range of interest for this material for the High Temperature Gas Cooled Reactor (HTGR) as well as the VHTR. The only current alternative is, thus, a full inelastic analysis requiring sophisticated material models that have not yet been formulated and verified. An additional impediment to the use of full inelastic analysis is the level of expertise and experience required to implement these models and interpret the results.

To address the prohibition on the use of current methods at very high temperatures, proposed code rules have been developed using elastic-perfectly plastic (E-PP) analysis methods that are expected to be applicable to very high temperatures. To provide data to implement the proposed rules and to verify their application, a series of tests have been initiated. One test concept, called a Simplified Model Test (SMT) (Jetter, 1998), takes into account the stress and strain redistribution in real structures by including representative elastic follow-up characteristics in the test specimen. Although the initial priority for the SMT approach is to generate data to support validation of the E-PP Code Case for evaluation of creep-fatigue damage, the broader goal of the SMT approach is to develop a methodology for evaluation of creep fatigue damage that is simpler to implement than the current complex rules and applicable to the full temperature range from ambient conditions to the very high temperature creep regime. There was also strategic direction from the ASME Code committee that, to the extent feasible, the E-PP Code Cases should be applicable to all current NH materials and not just the Alloy 617 Code Case. To support this, testing was conducted on 316H and 304H stainless steel to verify applicability to a broader range of materials.

During this reporting period, different specimen materials were tested under various loading conditions to provide data for validation of proposed E-PP Code Cases and to investigate whether the results were consistent and if they followed expected patterns of behavior. Most of the testing was accomplished using the basic solid bar specimen configurations with a nominal transition radius and elastic follow-up characteristic.

Tests were also initiated on cylindrical specimens design to be compatible with a test setup designed to accommodate test specimens with the follow-up characteristics to provide an upper bound of actual components. During testing of the “standard” SMT specimens, there was a problem dealing with the need to have a long, larger diameter, “driver section” to achieve higher, bounding values of elastic follow-up, in order to cause failure to occur in the shorter, narrower “test section” and to meet the requirement for a uniform temperature throughout the active length of the specimen. The problem occurred because the specimens sized to have a uniform temperature did not have enough available driver length to achieve the desired follow-up characteristics to envelope the response of actual components. This was exacerbated by the need to provide a generous transition radius between the narrower test section and the larger diameter driver section to avoid failure at the stress concentration at the start of the transition radius. Failure at the transition radius does not compromise the use of the data for validating the E-PP Code Cases. This is because the E-PP Code Case is applicable to any geometry, so in that sense, the transition radius is just another geometric variable to account. On the other hand, it does impact the use of the data for the longer

term goal of design curve development because the design curve logic is based on failure in the test section.

To address this issue, a modified SMT approach with a new type of specimen designated as the YSMT was developed to meet the multiple goals of uniform test temperature, failure in the test section and adequate bounding follow-up. Simply put, the YSMT specimen uses active control of a scaled driver section displacement in conjunction with the measured displacement in the test section to achieve the equivalent behavior of a standard SMT specimen. This approach also permits a generous transition radius to promote failure in the test section. Initial tests have been undertaken during the last reporting period to demonstrate the feasibility of the YSMT approach. Further YSMT testing identified a problem with buckling of the solid bar type specimens that was resolved by optimizing the design of a cost effective tubular specimen.

In this report, key points as related to the test program will be highlighted and summarized. The various SMT test article designs will be discussed along with the test results and the comparison between the EPP Code case predictions and experimental data.

2. SMT METHODOLOGY

A comprehensive discussion of elastic follow-up and the basis for the SMT methodology was included in the prior progress reports ORNL/TM-2012/428 (Sham, et al., 2012) and ORNL/TM-2013/349 (Wang, et al., 2013). That detailed discussion will not be repeated here, although the key points as related to the test program will be highlighted and summarized.

The SMT methodology is based on an elastic follow-up characterization of stress and strain redistribution due to creep. Suitably sized specimens based on elastic-follow-up concepts are cycled to failure and the data generated is used to develop a cyclic design curve for actual components.

2.1 ELASTIC FOLLOW-UP

Elastic follow-up can cause larger strains in a structure with displacement-controlled loading than would be predicted using an elastic analysis. Referring to Fig. 1, elastic follow-up may be quantified by computing the ratio of ε_{0-2} , the creep strain in the test section including elastic follow-up, to the creep strain that would have occurred under pure relaxation, ε_{0-1} . Thus, the elastic follow-up, q , is given by:

$$q = (\varepsilon_{0-2}) / (\varepsilon_{0-1}) \quad (1)$$

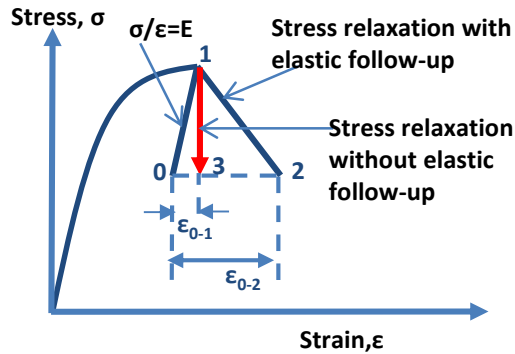


Fig. 1. Definition of elastic follow-up.

2.2 CONCEPTUAL BASIS OF SMT APPROACH

The basic concept of the SMT methodology is shown in Fig. 2. The component design is represented by a stepped cylinder with a stress concentration at the shoulder fillet radius. The component has a global elastic follow-up, q_n , which is due to the interaction between the two cylindrical sections, and a local follow-up, q_L , which is due to the local stress concentration.

If the thick cylinder is displaced radially inward a fixed amount, δ_{comp} , there will be a maximum strain at the area where stress concentration occurs. Although the actual strain may be higher, the relevant parameter in this approach is the maximum elastically calculated strain in the component, $\varepsilon_{E, comp}$. The effects of plasticity, creep and strain redistribution are accounted for in the simplified model test simulation.

Fig. 2(a) illustrates the damage from a strain, $\varepsilon_{E, comp}$, that is applied, held, and then cycled back to zero and reapplied. The damage is evaluated from a design curve, Fig. 2(b), based on data from the simplified model test, Fig. 2(c). The evaluation procedure is essentially the same as that used in Subsection NB, where the damage fraction is determined as the ratio of actual number of cycles, n , to the allowed number of cycles, N . The design curve envelopes the effects of hold time duration and follow-up magnitude without being excessively conservative. It is developed from SMT data that is plotted as elastically calculated strain vs. observed cycles to failure, Fig. 2(b). The two-bar SMT specimen is sized to envelope the follow-up characteristics of interest.

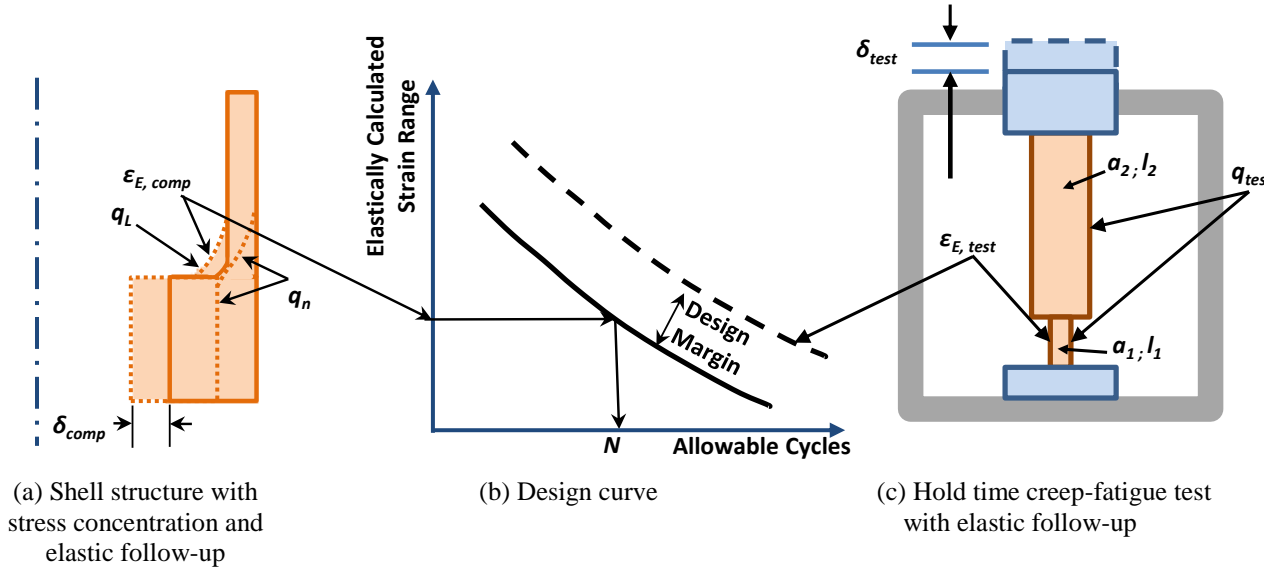


Fig. 2. SMT methodology.

A key point in the SMT approach is the use of elastically calculated strain in the test specimen to correlate the test results. The idea is that if, for the same elastically calculated strain, the effects of plasticity, creep and strain redistribution in the SMT specimen result in a stress-strain hysteresis loop that envelopes the hysteresis loop in the component, then the SMT results can be used to assess the cyclic damage in the component. A design margin must be applied to the test data to account for factors such as data scatter and extrapolation to longer hold times.

2.3 SMT SPECIMEN CHARACTERISTICS

In order to be effective, the SMT specimen must be sized to provide a stress-strain hysteresis loop under cyclic loading which envelopes the hysteresis loop of components of interest. Unfortunately, there is apparently no rigorous way to demonstrate that a two-bar model, Fig. 2(c), can bound the response under all circumstances. However, there are approaches based on a four-bar model representation of the stepped cylinder shown in Fig. 2(a) that can be used to demonstrate that the bounding strategy is applicable to a range of practical circumstances.

There are two types of geometric limitations. The first is the allowable value of local stress concentration when combined with the effects of global elastic follow-up. By requiring that the stress at the local stress concentration relax and using an expression for the relaxation rate developed by Kasahara

et al. (1995), Jetter (1998) developed the following restriction on elastic stress concentration, K , as a function of global follow-up q_n :

$$K \leq \frac{q_n}{q_n - 1} \quad (2)$$

There are two important reasons to avoid the regime where the stress in the local stress concentration is not relaxing. First, a high stress concentration in an area where there is a structural discontinuity with large global elastic follow-up can result in a nonlinear increase in localized strain range and accelerated creep damage. The second reason is that when the global follow-up becomes very large, it is not possible to bound the response with a reasonably sized SMT specimen. In our earlier Finite Element Analysis (FEA) (Wang, et al., 2013), K is defined as the ratio of the maximum principle stress at the stress concentration location to the average stress at the necked test section.

The second issue on geometric limitations is the magnitude of global follow-up, q_n , in the representative structure and the requirement that places on the follow-up of an SMT specimen in order to bound the response of representative structures of interest. As discussed by Jetter (1998), there have been numerous investigations reported in the literature. In summary, it appears that the value of global follow-up is conservatively represented by $q_n = 2$ and certainly bounded by a value of 3, provided that the stress range is suitably limited.

Based on the relaxation rate expression of Kasahara et al. (1995), Jetter (1998) developed an expression for the peak combined follow-up, q_p , in the four-bar structure given by:

$$q_p \leq Kq_n \quad (3)$$

for a range of practical values of K and q_n . This expression for peak elastic follow-up was also recommended by Takahura et al. (1995), based on thermal transient testing of a cylindrical shell using a notch model and a stepped cylinder model.

Combining Eqs. (2) and (3) with the global follow-up of representative structures results in the following requirement for the follow-up of an SMT specimen in order to bound the response of representative structures of interest;

$$q_p \leq 4.0 \text{ to } 4.5 \quad (4)$$

This follow-up value is the target value for developing a SMT design curve.

2.4 YSMT DEVELOPMENT AND VERIFICATION

The overall rationale and characterization of the YSMT approach was described in the prior progress report, Wang et.al. (2014). However, for continuity, an abridged version of that discussion will be repeated here. During testing of the “standard” SMT specimens, there was a problem dealing with the need to have a long, larger diameter, “driver section” to achieve higher, bounding values of elastic follow-up, in order to cause failure to occur in the shorter, narrower “test section” and to meet the requirement for a uniform temperature throughout the active length of the specimen. The problem occurred because the specimens sized to have a uniform temperature did not have enough available driver length to achieve the desired follow-up characteristics to envelope the response of actual components.

An alternative approach has been identified through the use of a two-segment control scheme that mimics a much longer driver section through electronic amplification of the displacement of a relatively short driver section. For convenience, this approach has been identified as the YSMT configuration. The conceptual basis for the YSMT approach is illustrated in Fig. 3.

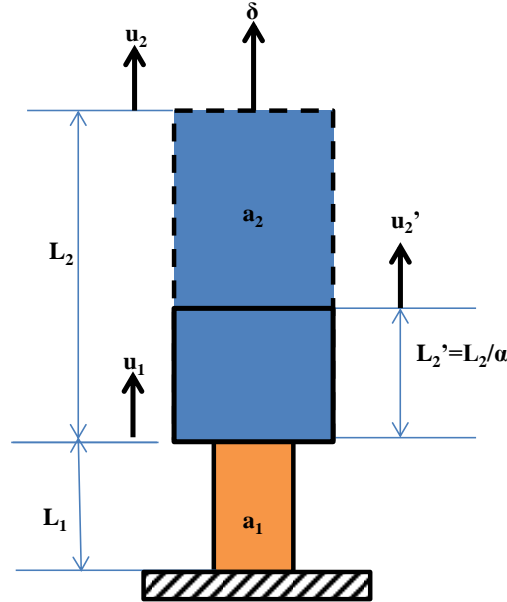


Fig. 3. YSMT test concept.

L_1 , a_1 and u_1 are the length, area, and displacement at the necked test section and L_2 , a_2 and u_2 are the length, area, and displacement at the driver section for the standard SMT specimen. The YSMT specimen has an identical necked test section but with a much shorter driver length of L_2' . The YSMT testing concept uses the specimen with shorter driver length of L_2' to produce equivalent test results as an original SMT specimen with a driver length of L_2 , where,

$$L_2' = \frac{L_2}{\alpha} \quad (5)$$

The SMT methodology is based on the cycles to failure at an elastically calculated strain in the test section for a given loading condition. In the YSMT model shown in Fig. 3, the displacement, δ , required to generate an elastically calculated strain is given by

$$\delta = L_1 \left[1 + \left(\frac{L_2}{L_1} \right) \left(\frac{a_1}{a_2} \right) \right] \quad (6)$$

For YSMT to generate the same results as the standard SMT configuration, the displacement u_2' and u_1 must be controlled such that:

$$\alpha u_2' + u_1 = \delta \quad (7)$$

To implement this YSMT concept, the displacement signal measured from the driver section u'_2 must be magnified by a factor of α , while keeping the displacement in the necked test section, u_1 , to be the same. Experimentally, this is achieved using two displacement measuring devices, and the devices are calibrated so that the displacement signal from the u'_2 is scaled with a factor of α .

The feasibility of this YSMT concept was demonstrated and verified using an SS316L specimen as reported in Wang, et al. (2013). However, that specimen did not have a high follow-up factor, q , which turned out to be a critical issue. When the solid bar specimen was tested at a bounding follow-up, buckling problems were encountered which resulted in the use of a tubular specimen which has greater inherent buckling resistance than a solid bar specimen.

3. TEST DESCRIPTION

The objectives of the test program are to generate experimental data to (a) provide a basis for verification of the EPP methodology for evaluation of creep-fatigue damage of both current NH materials and the proposed inclusion of Alloy 617, (b) verify the constitutive equations supporting inelastic analysis of Alloy 617, and (c) support development of the SMT design methodology. To maximize resources, the use of currently available testing components, i.e., loading frames, heaters and measurement systems, was emphasized. To provide a link to ongoing creep-fatigue studies at the Idaho National Laboratory and to minimize material procurement time and expense, it was decided to use the same Alloy 617 plate material for the current program as what is being used for standard creep-fatigue testing at Idaho National Laboratory (INL).

There was also a strategic direction from the ASME Code committee that, to the extent feasibility, the E-PP Code Cases should be applicable to all current NH materials and not just the Alloy 617 Code Case. To move in this direction, testing was included on 304H and 316H stainless steel to verify the design methodology's applicability to a broader range of materials.

3.1 MATERIALS

3.1.1 Alloy 617

To support this study, the Idaho National Laboratory supplied an Alloy 617 plate, Heat 314626 from ThyssenKrupp VDM USA, Inc., with dimensions of 30"×69"×1.5". The plate allows one of the SMT solid bar specimens or tubular specimen to be prepared in the thickness direction with the given diameter of specimen as will be discussed below.. The chemical composition of the plate is listed in Table 1. The specimen longitudinal direction is lined up with the rolling direction of the plate (schematically shown in Fig. 4).

Table 1. Chemical compositions of Alloy 617 plate with heat number 314626 (weight %)

C	S	Cr	Ni	Mn	Si	Mo	Ti	Cu	Fe	Al	Co	B
0.05	<0.002	22.2	R54.1	0.1	0.1	8.6	0.4	0.04	1.6	1.1	11.6	<0.001

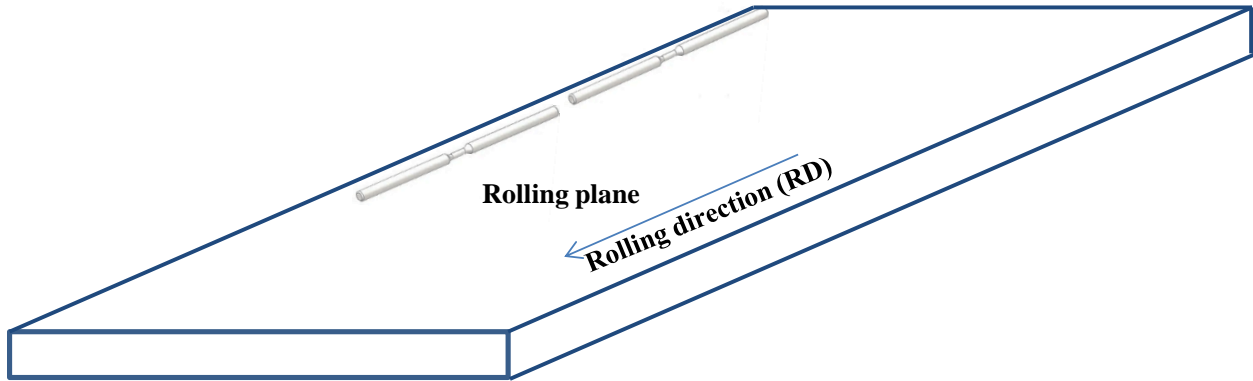


Fig. 4. Schematic of the layout of the specimens on the Alloy 617 plate.

The microstructural characteristics of the Alloy 617 plate for the rolling plane and the transverse planes were presented in a previous progress report, ORNL/TM-2013/349 (Wang, et. al, 2013). No significant differences in grain size distribution were observed across the thickness. The microstructure of the cross-sectional plane normal to the rolling direction is shown in Fig. 5.

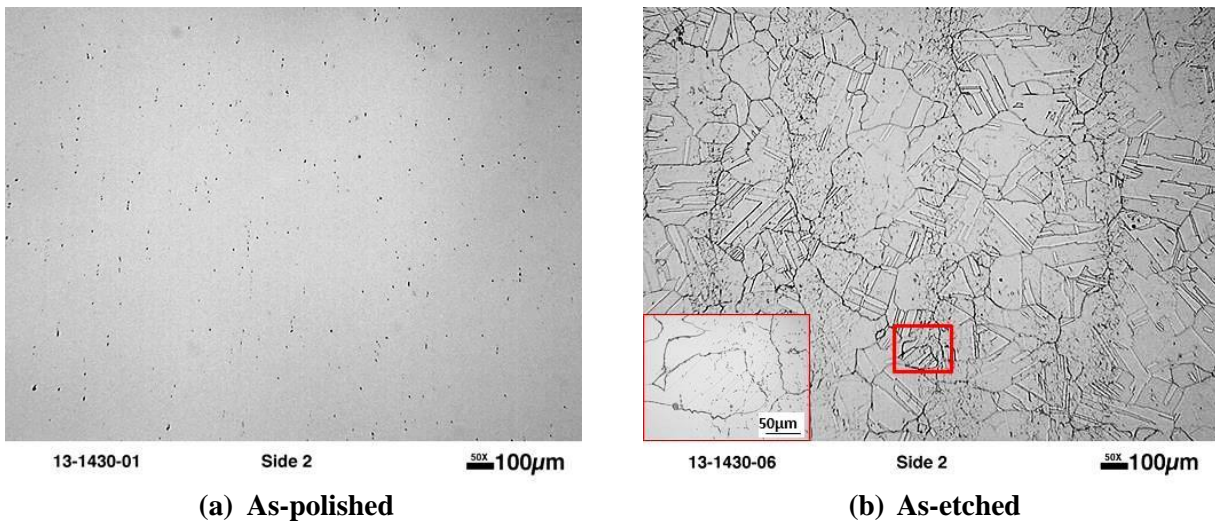


Fig. 5. Optical images of the as-received Alloy 617 plate for the cross-sectional plane normal to the rolling direction.

4.1.2. Stainless steel 304H

SS304H round bar material with nominal diameter of 1 in was purchased from Outokumpu Stainless Bar, LLC. The heat number is E131181 and the as-received SS304H bar satisfies specification ASME SA497/A479M 13b. The chemical composition of the SS304H is listed in Table 3.

Table 2. Chemical compositions of SS304H bar with heat number E131181 (weight %)

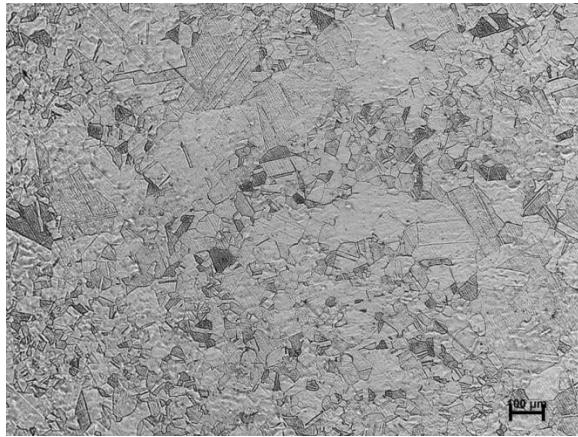
C	P	Si	Ni	Mn	N	Ti	Sn	V	Fe	Cb-Ta
0.048	0.033	0.300	8.300	1.870	0.080	0.002	0.006	0.060	balance	0.020
Ta	S	Cr	Co	Mo	Cb	Al	W	Cu		
0.10	0.025	18.270	0.173	0.250	0.010	0.005	0.020	0.260		

3.1.2 Stainless steel 316H

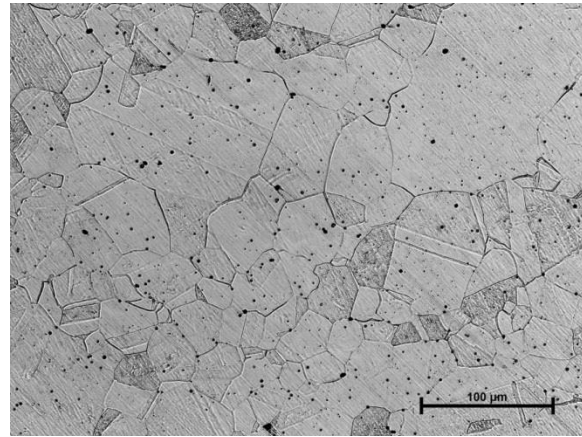
SS316H round bar material with nominal diameter of 1 in was purchased from Outokumpu Stainless Bar, LLC. The heat number is 101076 and the as-received SS316H bar satisfies specification ASME SA497. The chemical composition of the SS316H is listed in Table 3. The microstructure of the cross-sectional plane for the SS316H is shown in Fig. 6 (only near center about 0.5 in diameter is shown). Bimodal grain size distribution with the grain sizes of ~50um and 300um was observed.

Table 3. Chemical compositions of SS316H bar with heat number 101076 (weight %)

C	P	Si	Ni	Mn	N	Ti	Sn	V	Fe	Cb-Ta
0.045	0.028	0.650	10.120	1.420	0.053	0.002	0.006	0.060	balance	0.014
S	Cr	Co	Mo	Cb	Al	B				
0.024	16.230	0.279	2.090	0.014	0.004	0.004				



(a) Optical image at 50X



(b) Optical image at 200X

Fig. 6. Optical images of the as-received SS316H.

3.2 SPECIMEN SIZING

Although not a strict requirement for establishing design curves (the correlation is based on elastically calculated strain, not actual measured quantities), strain measurements provide insight into the role of follow-up in strain redistribution and support the use of SMT results in the development and verification of constitutive models for detailed inelastic analysis. The necked test section of the SMT specimen requires about 0.5 in axial length for local strain measurement.

Sizing of the SMT specimen to achieve a specified follow-up, q , was based on the approximation for a two-bar model developed by Kasahara et al. (1995) as shown in the following equation, which has been simplified to represent a single material

$$q = \left[1 + (l_2 / l_1)(a_1 / a_2) \right] / \left[1 + (l_2 / l_1)(a_1 / a_2)^m \right] \quad (8)$$

where l_1 and a_1 represent the area and the length of the shorter, higher stressed section (shown in Fig. 2c); l_2 and a_2 represent are the area and length of longer, lower stressed member (Fig. 2c); and m is the material creep rate exponent.

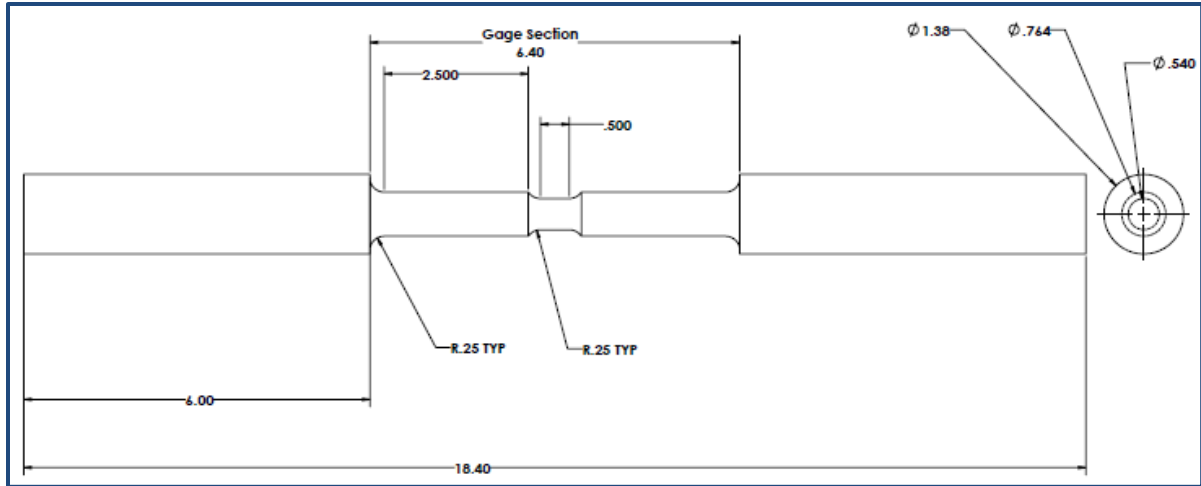
To maximize the follow-up factor, q , for a given specimen length, an area ratio of approximately 0.4 – 0.5 is desirable. For Alloy 617 specimens, based on an area ratio of $a_1 / a_2 = 0.5$, a length ratio of $l_2 / l_1 = 9$ and a power law creep exponent of $m = 6$, the resultant value of q is about 4.8. However, it is difficult to estimate the effect of the transition lengths from thick to thin sections using the approximate relationship in Eq. (8) although the effect will be to decrease the elastic follow-up parameter. If possible, it would be advantageous to minimize the stress concentration at the change in diameter to ensure that the failure occurred in the uniform diameter as opposed to the transition radii. However, this limits the achievable elastic follow-up factor because there was a) an initial length limitation due to furnace availability and b) a concern about lateral stability of the specimen under compressive loading.

3.2.1 SMT specimen design

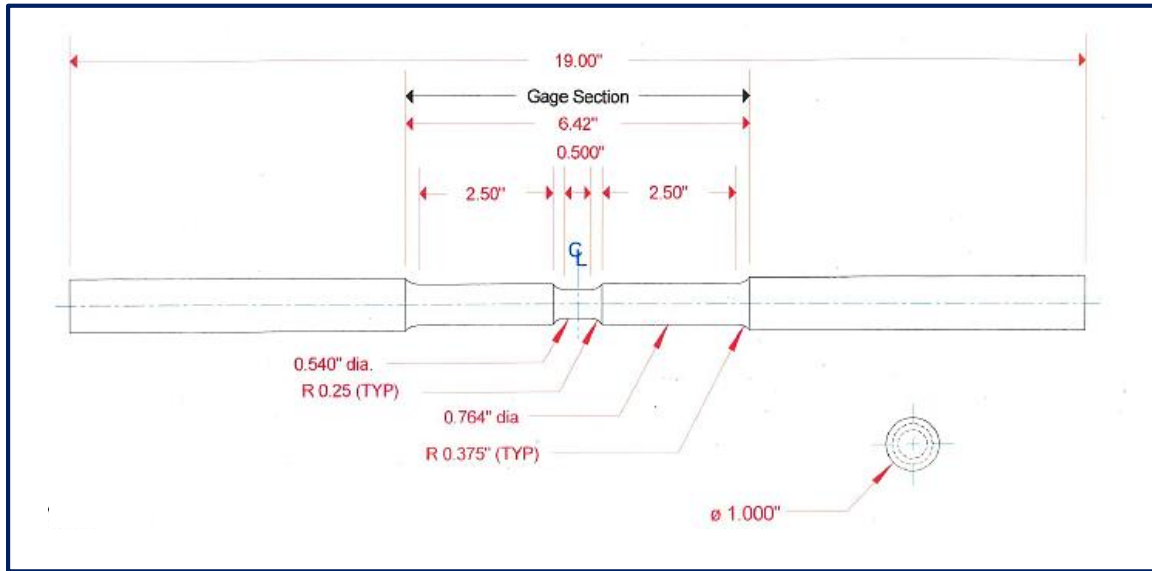
Due to the high machining cost of tubular specimens out of solid plate for Alloy 617, it was decided to change to much less expensive solid bar specimens to generate SMT creep fatigue data to support ASME Code Case approval. Finite element analyses (FEA) using an elastic model were conducted to reach a compromise, with the resultant configuration shown in Fig. 7(a). The resultant stress concentration at the toe of the transition radius was calculated to be $K = 1.37$. This is the Type 1 SMT solid bar specimen geometry. A more comprehensive presentation of this study appears in Sham et al. (2012). There was an initial effort to increase the transition radius to 1.08in and therefore lower the stress concentration factor to 1.09 (Wang, et al., 2013) in order to increase the chance of failure inside the uniform necked test section. Although a larger elastic follow-up factor was achieved, the results showed that the failure location was still at the toe of the transition radius. In addition, the increase in the specimen total length due to the addition of the transition length was large and exceeded the uniform temperature zone of the heating source. The non-uniform temperature distribution in the driver section also raised uncertainties when performing FEA. Therefore, the decision was to stop further testing for this large transition radius SMT specimen geometry.

The Type 1 geometry for Alloy 617 was based on a maximum isothermal specimen length and a test or necked test section diameter-sized to provide the same radius of gyration as the tubular specimen to provide equivalent protection against a buckling failure mode. The driver section diameter was sized to provide an area ratio of 0.5 to maximize the follow-up factor within a given specimen length. The transition radius of 0.25in was selected based on elastic analysis of the stress concentration to provide the lowest stress concentration consistent with the overall length constraint and the necked test section length required for the extensometer. The hope was that the specimen failure would occur in the gage section and not at the transition radius, although this turned out not to be the case.

The Type 1 geometry was also used for SS304H and SS316H specimens. The details of the gage length section for SS316H and SS304H are identical to the Type 1 geometry for Alloy 617. Specimen geometries for Type 1 SMT specimens are shown in Fig. 7.



(a) Type 1 SMT geometry for Alloy 617



(b) Type 1 SMT geometry for SS316H and SS304H

Fig. 7. Type 1 SMT solid bar specimen design.

The basic specimen dimensions and control parameters related to achieve different combinations of Stress Concentration Factor (SCF) and target elastic follow-up factor (q) are summarized in Table 4.

Table 4. SMT testing specimen geometry

	Necked test section length, in	Transition radius, in	SCF	Transition length, in	Driver section length, in	Total testing length, in	Target q value	Material Tested
Type 1	0.5	0.25	1.37	0.208	4.08	5	3.5	Alloy 617, 304H, 316H

3.2.2 YSMT Specimen Design

To ensure a buckling safety design for YSMT, tubular YSMT and SMT testing, a series of buckling simulations were conducted using ABAQUS finite element analysis software before the sample preparation. The geometric drawings of YSMT, tubular YSMT and SMT are listed in the left column of Fig. 8 with enumerated as (a), (b) and (c) respectively. The corresponding numerical models are listed with same order in the right column of Fig. 8. In the geometric drawings, some sections are for gripping section, which is not effective for the buckling analysis. The effective length for buckling analysis is sketched as the section between the red dashed lines.

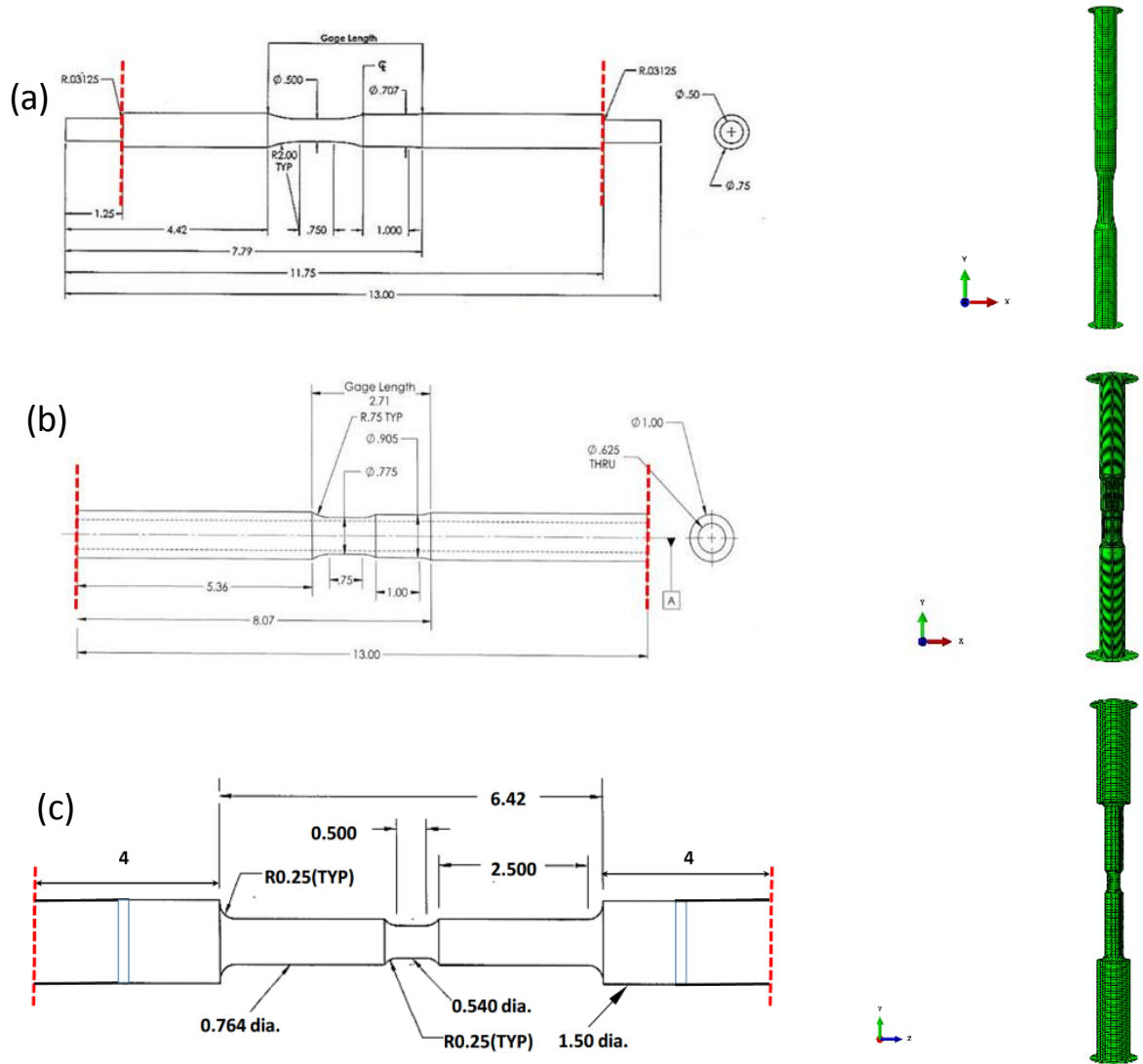


Fig. 8. (a) YSMT, (b) tubular YSMT and (c) SMT configuration and corresponding FEA model

Two rigid planes are added at both ends of each simulation model with only Y displacement freedom unconstrained for bottom plane and all displacement degrees of freedom constrained for top plane. The

angular rotations in all directions are constrained to ensure that an axial loading force can be applied to the model evenly. A unit force is applied to the bottom plane and a buckling analysis step is conducted to get the first modal eigenvalue. The critical loading force is evaluated with the value of unit force timing first modal eigenvalue. The critical buckling loads for three types of geometries are tabulated in Table 5. Since stress in testing section is critical in studies, the corresponding stress values are also tabulated. These results are not intended to be a prediction of the absolute load to buckle but, rather, a prediction of the relative buckling resistance since the effects of plasticity and creep were not accounted. Note that the Tubular YSMT specimen has much greater buckling resistance than the original solid bar specimen and somewhat greater resistance than the SMT specimen which did not encounter buckling issues.

Buckling patterns for each model are also shown in Fig. 9. Note the triad directions are different for three contour plots, and the directions have been shown at left bottom corners.

Table 5. Buckling load and stress values for each model

Model Name	Area (inch ²)	Buckling load (kip)	Buckling Stress (ksi)
Solid YSMT	0.196349541	60.0	305.7
Tubular YSMT	0.164933614	160.8	975.1
Standard SMT	0.229022104	212.7	928.6

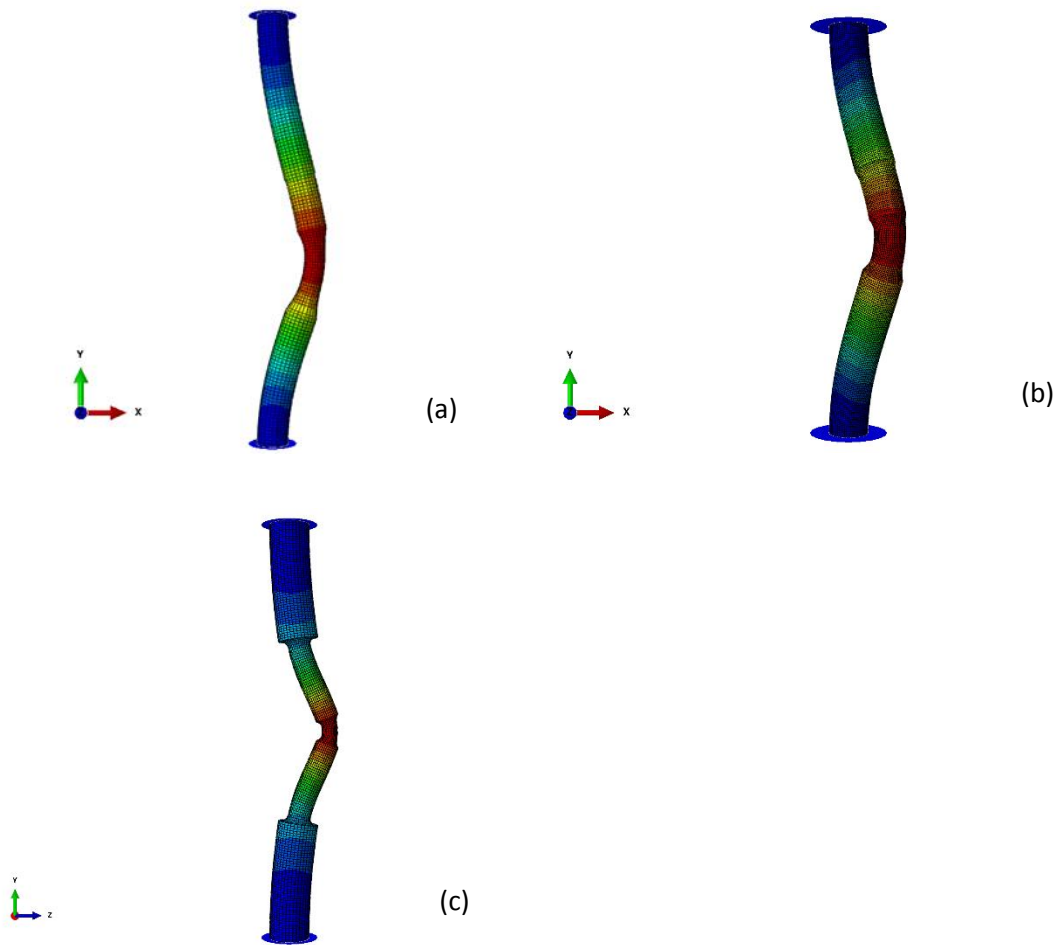


Fig. 9. Buckling contour plot for (a) YSMT, (b) tubular YSMT and (c) SMT models

The final YSMT specimen configuration, which did not buckle on test, is shown below in Fig. 10.

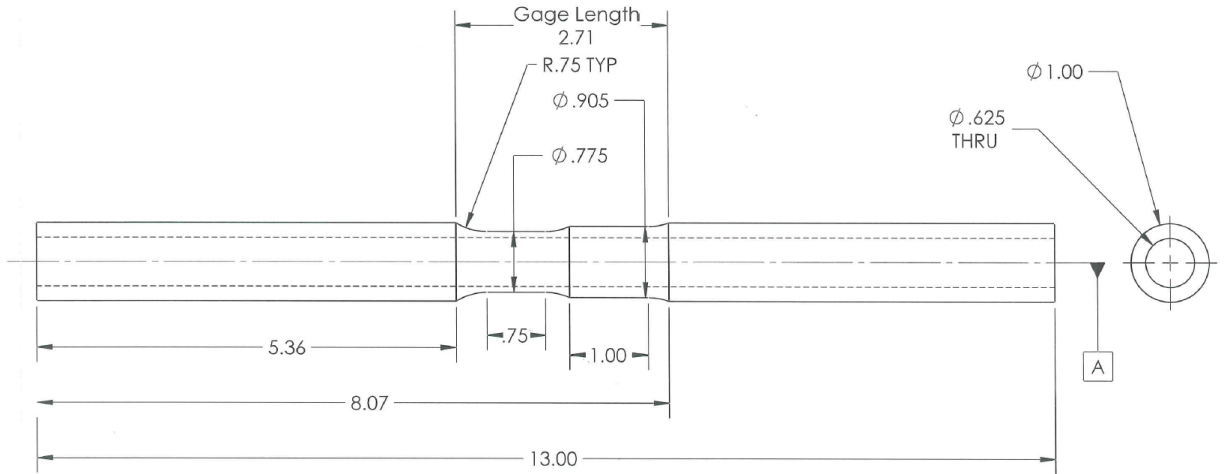


Fig. 10. YSMT test specimen configuration

3.3 EXPERIMENTAL SETUP

3.3.1 SMT Testing and Instrumentation

The creep-fatigue testing on both Alloy 617 and SS304H/SS316H were performed on servo-hydraulic test machines. Tests used a fully reversed loading profile with holding time at peak tension. A schematic of the loading profile is show in Fig. 11; loading was automated through a LabView program.

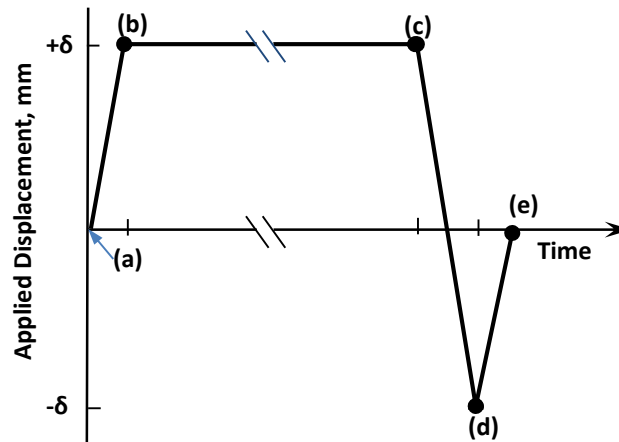


Fig. 11. Applied end-displacement profile for one cycle of creep-fatigue testing.

A three-zone resistance furnace was used to reach uniform temperature along the specimen. Multiple type S thermo-couples were attached to the specimen surface using platinum wires to monitor the

temperature along the length and around the circumference throughout the test. The maximum temperature difference across the gage section satisfies the ASTM E2714 – 09 requirement of less than 1% of the target testing temperature. A picture of the test system is shown in Fig. 12.

SMT method requires testing a specimen with accurate end displacement control. This type of accuracy is not achievable using the machine stroke, so in this study the accurate end displacement control was accomplished using a modified extensometer. For the conditions with different l_2 to l_1 length requirements, the gage length of the extensometer will have to be adjusted accordingly. An extensometer with original gage length of 1in was adapted and extended with different gage lengths to support desirable testing lengths for different SMT specimen types. The extensometer probes in contact with the specimen surface are made of high purity alumina rods. The control extensometer was calibrated to have an output of 10 volts for an extension of 0.02 in with a class B1 specification (ASTM E83 – 10a). The entire controlled testing section includes the 0.5 in long necked test section l_1 , a transition length from l_1 to l_2 section, and a thicker driver section l_2 . The tests were then performed using a control mode through this extensometer with extended gage length, and an accurate end displacement is therefore achieved through this control mode. In addition, it should be noted that the transition length is not considered in the analytical calculation using Eq. (8). The addition of the transition length is necessary, and the purpose was to have the test specimen fail within the necked test section.

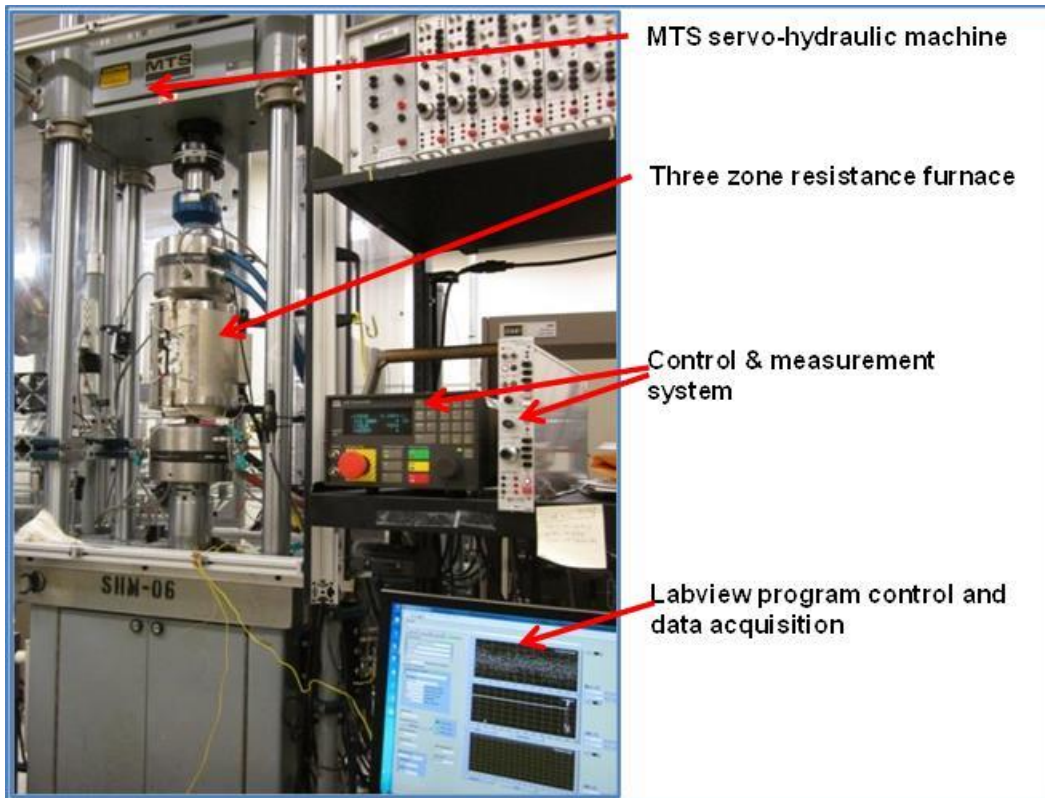


Fig. 12. SMT test system.

A second extensometer with a gage length of 0.4 in was used to measure the strain signal in the l_1 necked test section. The measurement extensometer was verified to be class B2 (ASTM E83 – 10a). The stress response for the necked test section was calculated as the total load divided by the original cross-sectional area. Therefore, stress-strain hysteresis loops can be generated for this necked test section. The

stress and strain information collected from this necked test section will show the elastic follow-up effect and can be used for verification of material constitutive models for inelastic analysis.

3.3.2 YSMT Testing System

The YSMT method uses the combined signal from two extensometers to control specimen deformation and achieve creep-fatigue testing with a designed elastic follow-up factor. The calibration values of the two extensometers are different. The output signal of the extensometer on driver section is magnified to a desired value to represent a long driver length. The experimental setup for YSMT is shown in Fig. 13. The extensometer at the necked test section has a gage length of 0.5in, and the one on the driver section is 0.75in. The designed parameters for YSMT are summarized in Table 6.

Based on the analytical calculation in Eq.(8), this set of parameters will generate testing results with an elastic follow-up factor of 4.3 using creep component $m = 6$. The redistribution of the strains between the driver section and the necked test section causes the specimen ratchet during YSMT creep-fatigue experiments. Large ratcheting strains in the necked test section will cause the extensometer probes to pop off the specimen. Since both extensometer signals are combined and used for control of the testing, either one of the extensometer probes popping off the specimen will immediately result in failure of the specimen. In order to resolve this issue, an automated Z-stage was installed to accommodate the ratcheting of the extensometer at the necked test section. The Z-stage is controlled by LabView software and automatically recognizes the amount of the ratcheting strain for each cycle and makes corresponding adjustments to prevent extensometer pop-off.

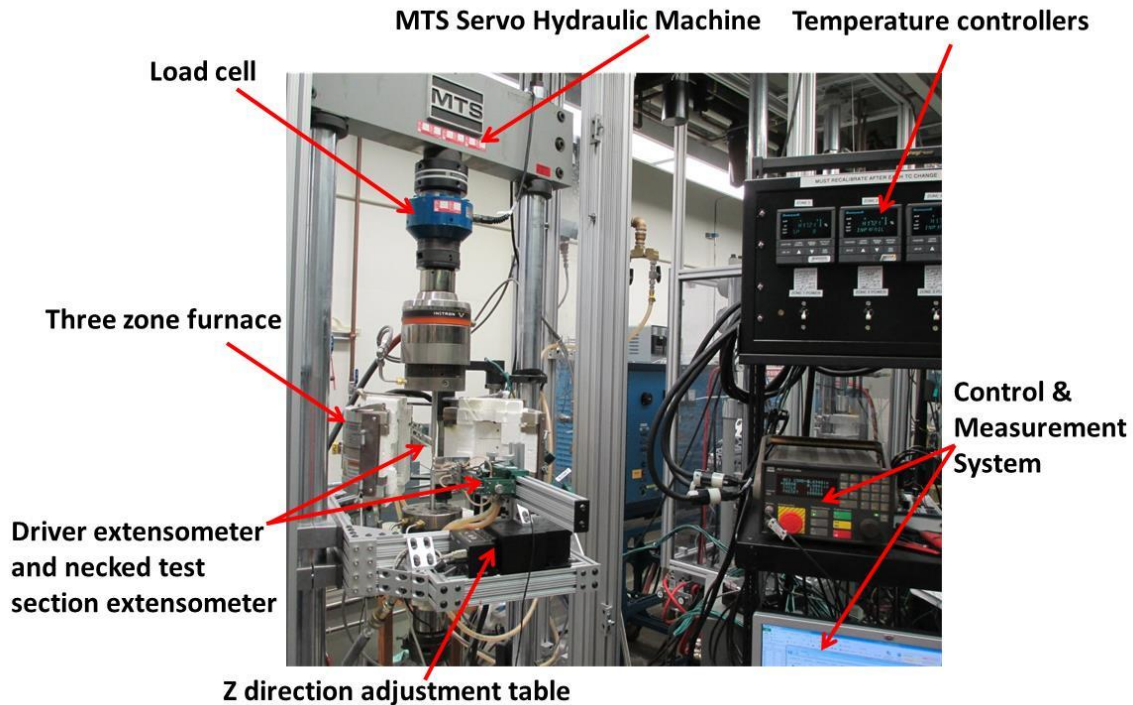


Fig. 13. The YSMT system.

Table 6. YSMT parameters

Necked test section extensometer gage length	Necked test section extensometer output for 10 volt	Driver section extensometer gage length	Drive section extensometer output for 10 volt	Represented driver section length	Target q value	Material Tested
0.5 in	30 mils	0.75 in	6 mils	3.75 in	4.5	SS316H

Page Intentionally Blank

4. TEST RESULTS

4.1 SMT CREEP-FATIGUE OF ALLOY 617

Four Type 1 SMT specimens were tested for Alloy 617. Tests performed and the basic test parameters are summarized in Table 7. Also shown (shaded) for comparison are the test results from the prior reporting period. Defining the cycles to failure is somewhat subjective since deviation from established steady state behavior is judged to be more relevant than actual specimen separation. Generally, deviation from the steady state behavior of the maximum and minimum stress and cyclic strain range are the pertinent variables considered. The cycles to failure is defined as the cycle number where the maximum and minimum stress and the strain range deviated from the steady state.

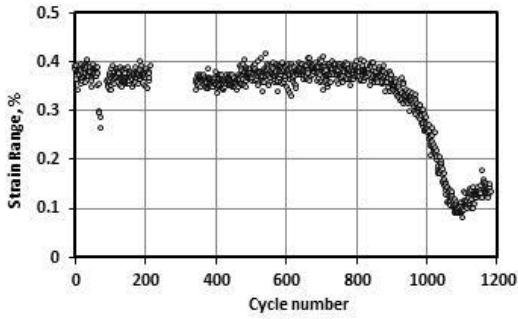
In the following sections, representative test results will be presented for the three test geometries. The elastic calculated strain ranges in the necked test section and at the notch are from FEM according to the ASME NH procedure. Our earlier report summarized the characteristics of the Type 1 and Type 2 SMT for Alloy 617 (Wang, et al., 2013).

Table 7. SMT creep-fatigue for Alloy 617

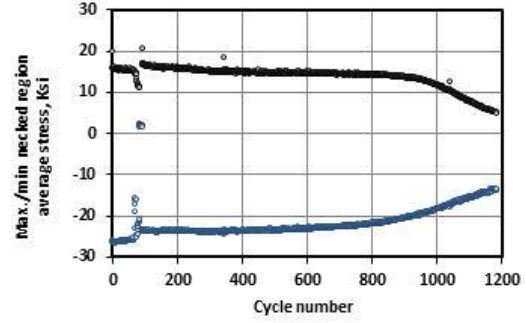
Specimen Type	Test No.	Specimen ID	Amplitude, δ value in Fig. 11	Elastic calculated strain range inside gage	Hold time, s (b)→(c); Fig. 11	Initial strain range	Test temperature °C	Life time, h	Cycles to failure
Type 1	#1	R1C2	4.5 mil	0.296%	600	0.65	950	78.2	460
	#2	R2C1	4.5mil	0.296%	600	0.63	950	76.5	450
	#7	R11C2	2.9mil	0.196%	600	0.25	950	170	1000
	#10	R11C1	4.5 mil	0.296%	600	0.71	950	475	950
	#11	R16C3	1.8mil	0.121%	180	0.16	950	56	1050
	#17	R15C2	2.8 mil	0.196%	600	0.38	950	153	900
	#18	R21C4	2.85mil	0.196%	600	0.36	950	170	1000
	#21	R11C3	4.9 mil	0.339%	600(cycle>12) 200(cycle 1-12)	0.64	850	85.4	510
#22	R17C4	2.75 mil	0.183%	600(cycle>17) 200(cycle 1-17)	0.3	850	386	2280	
Type 2	#4	R6C2	2.75 mil	0.296%	600s	0.66	950	63	370
	#5	R6C3	2.75 mil	0.296%	600s	0.62	950	60	350
	#8	R7C2	1.8mil	0.194%	600s	0.31	950	160	940
	#9	R7C1	1.8mil	0.194%	600s	0.32	950	162	950
Tubular	#13	INC617-T1	4.5 mil	0.299%	600s	0.7	950	20	120
	#16	INC617-T3	4.5mil	0.299%	600s	0.72	950	37	220

Note: test#1-16 were previously tested and the specimen geometries for Type 2 and tubular were reported in Wang et.al. 2014

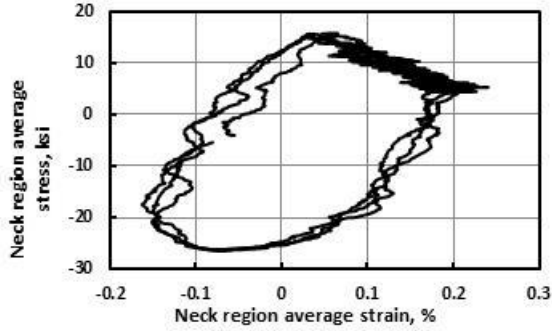
Shown below in Fig. 14 though Fig. 17 are plots of the measured strain range and maximum (tension) and minimum (compressive) stress as a function of cycle number, representative hysteresis loops and stress history for the above tabulated test conditions from this reporting period.



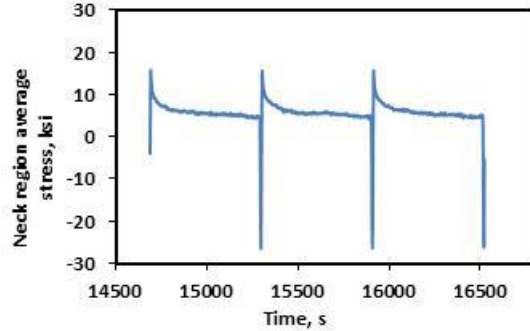
(a) Strain range



(b) Max/Min stresses

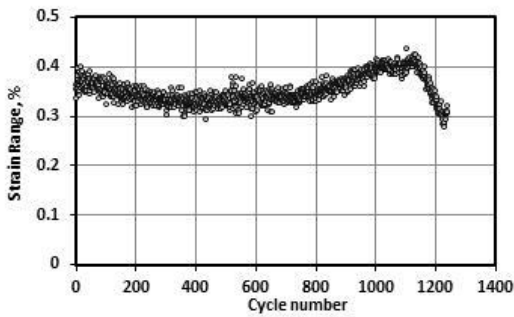


(c) Hysteresis Loop

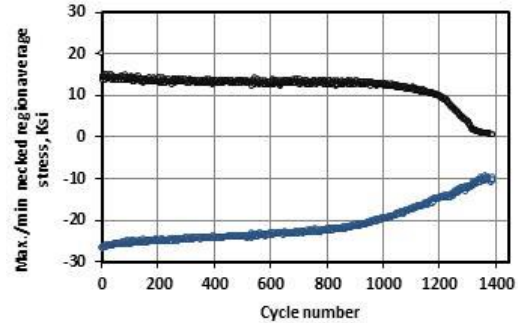


(d) Stress history

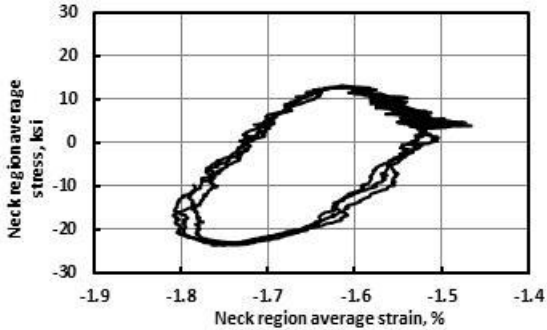
Fig. 14. Test results for test #17 (Alloy 617-950 °C)



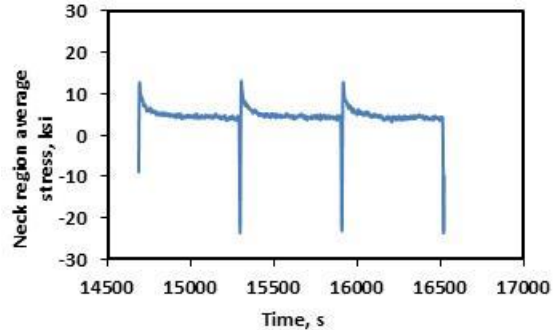
(a) Strain range



(b) Max/Min stresses

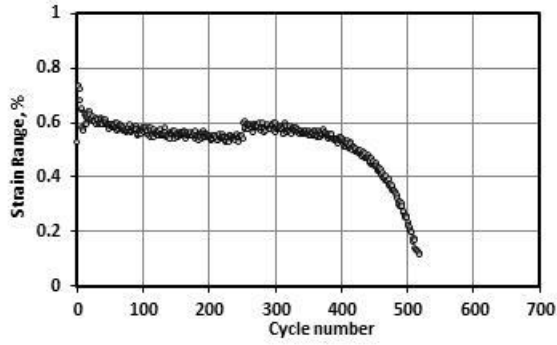


(c) Hysteresis Loop

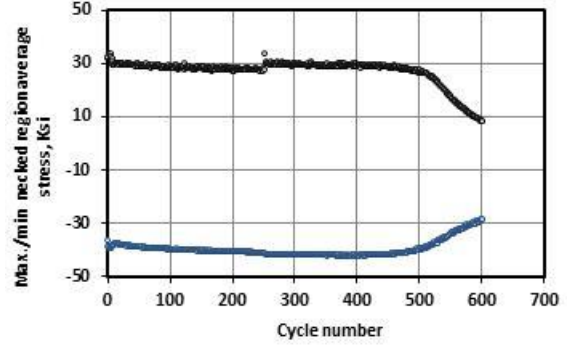


(d) Stress history

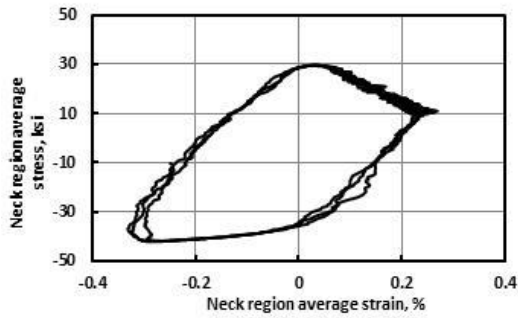
Fig. 15. Test results for test #18 (Alloy 617-950 °C)



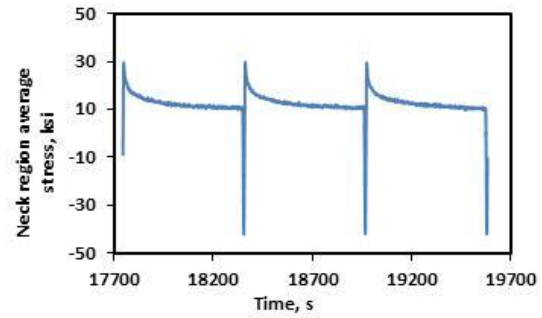
(a) Strain range



(b) Max/Min stresses

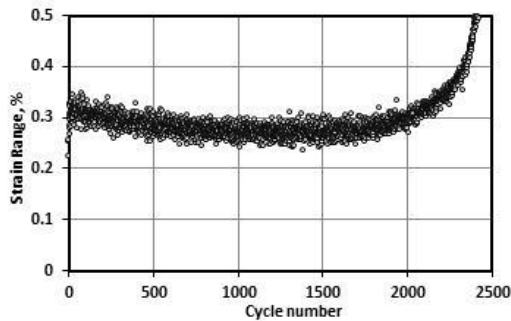


(c) Hysteresis Loop

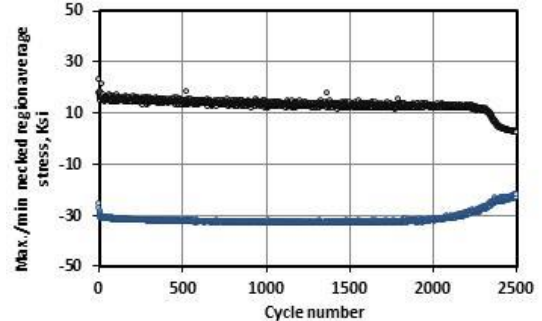


(d) Stress history

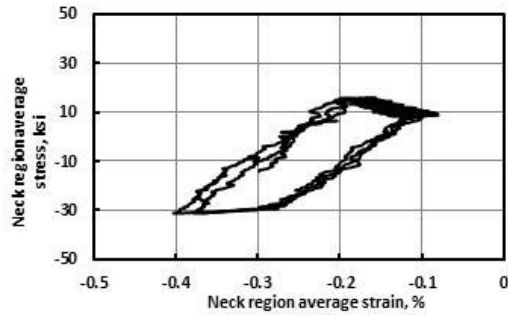
Fig. 16. Test results for test #21 (Alloy 617-850 °C)



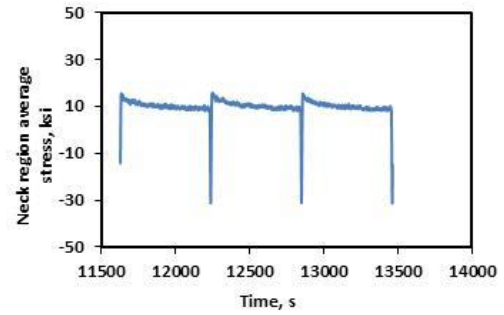
(a) Strain range



(b) Max/Min stresses



(c) Hysteresis Loop



(d) Stress history

Fig. 17. Test results for test #22 (Alloy 617-850 °C)

The above results show good agreement with expected trends. Tests #17 and #18, run at equivalent conditions (950°C and close to 0.4% strain range), show good agreement in cycles to failure, hysteresis loops and stress relaxation during the hold period. What is different is the measured strain range, roughly equivalent prior to failure but, at the onset of failure, Test #17 shows a decreasing strain range and Test #18 an increasing strain range. There is not yet a readily apparent reason for the difference but it does not seem to influence the observed life or behavior prior to failure.

Test #21 at a lower temperature but higher strain range has a longer life and also exhibits significant stress relaxation even at the lower temperature of 850°C. What is interesting is the comparison to Test #22 in which the stress relaxation is much slower. This is believed due to the much lower applied displacement amplitude, 2.75mil vs. 4.5mil, and the resultant lower stress at the start of the relaxation cycle, about 12ksi vs. 30ksi.

4.2 SMT CREEP-FATIGUE OF SS316H

Two Type 1 SS316H specimens were tested to failure, one at 815°C and the other at 650°C. Table 8 lists the testing parameters. For completeness, the SS316H specimen tested during the prior reporting period is also shown (shaded).

Table 8. SMT creep-fatigue for SS316H

Specimen Type	Test No.	Specimen ID	Amplitude, δ value in Fig. 11	Elastic calculated strain range inside gage	Hold time (b)→(c); Fig. 11	Initial strain range	Test temperature °C	Life time, h	Cycles to failure
	#15	SS316H-spec2	4.5 mil	0.296%	600	0.62%	815	70	410
Type 1	#19	SS316H-spec3	1.8 mil	.125%	600(cycle 1-4470) 180(cycle >4471)	0.17%	815	>1226	>13,214 Not failed
	#20	SS316H-spec4	5.7 mil	.375%	600(cycle>12) 60(cycle 1-12)	0.62%	650	172	1020

Note: test#15 was previously tested.

A close-up photograph of the prior test #15 specimen SS316H after testing is shown in Fig. 18. The specimen failed at the toe of the transition radius. After testing, the necked test section showed barreling, the diameter at the center increased from 0.54 to 0.565in, and oxide scales were also visible on the surface.

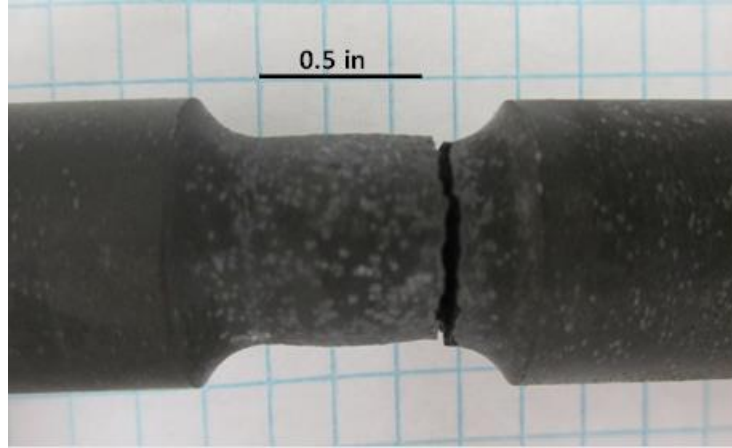


Fig. 18. Picture of SS316H after testing (from previous testing)

Shown below in Fig. 19 and Fig. 20 are plots of the measured strain range and maximum (tension) and minimum (compressive) stress as a function of cycle number, representative hysteresis loops and stress history for the above tabulated test conditions from this reporting period.

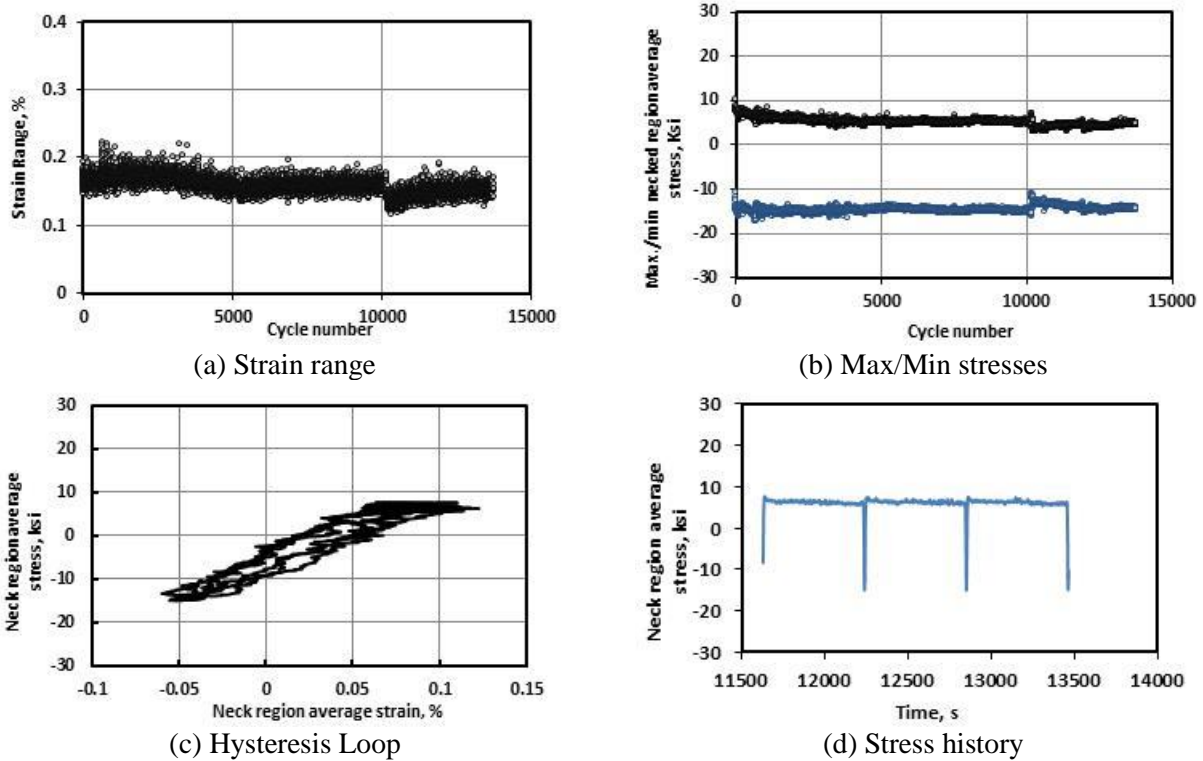


Fig. 19. Test results for test #19 (SS316H-815 °C)

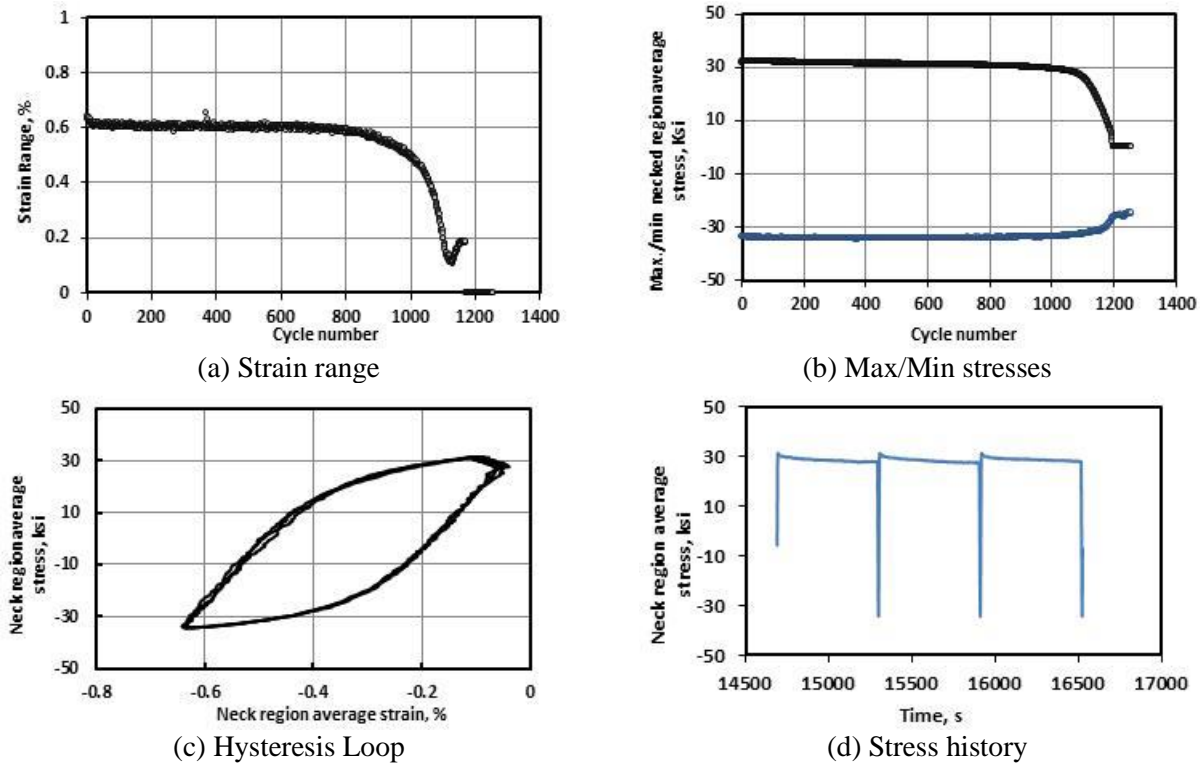


Fig. 20. Test results for test #20 (SS316H-650 °C)

Test #19 at 815°C lasted a long time, over 13,000 cycles, before the test was stopped. The long life at this temperature is attributed to the low applied displacement amplitude and low resulting strain range (0.175%) and stress (about 15ksi). As would be expected, the hysteresis loops were narrow with relatively little inelastic strain and there was little stress relaxation due to the low starting values. Test #20 at 650°C failed at about 1020 cycles but the strain range was much higher, 0.62%, and the hysteresis loops much wider due to plasticity. There was little stress relaxation during the cycle.

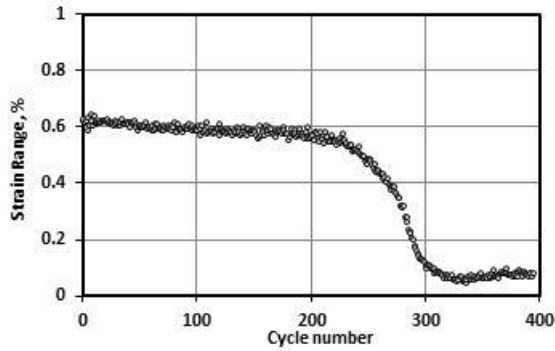
4.3 SMT CREEP-FATIGUE TESTING OF SS304H

Three Type 1 SS304H tests were run, two at 815°C and one at 650°C. Four Type 1 SMT specimens were tested for Alloy 617. The basic test parameters are summarized in the table below.

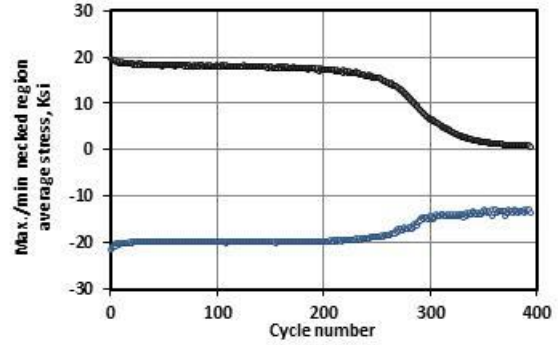
Table 9. SMT creep-fatigue for SS304H

Specimen Type	Test No.	Specimen ID	Amplitude, δ value in Fig. 11	Elastic calculated strain range inside gage	Hold time (b)→(c); Fig. 11	Initial strain range	Test temperature °C	Life time, h	Cycles to failure
Type 1	#24	SS304H-spec8	3.9 mil	0.257%	600	0.60%	815	66	390
	#25	SS304H-spec2	4.5 mil	0.296%	600	0.78%	815	29	170
	#26	SS304H-spec7	4.5 mil	0.296%	600	0.50%	650	264	1550

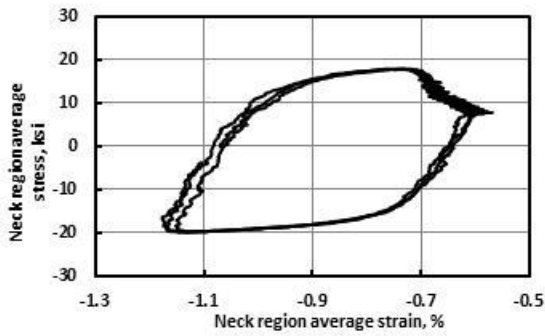
Shown below in Fig. 21 through Fig. 23 are plots of the measured strain range and maximum (tension) and minimum (compressive) stress as a function of cycle number, representative hysteresis loops and stress history for the above tabulated test conditions.



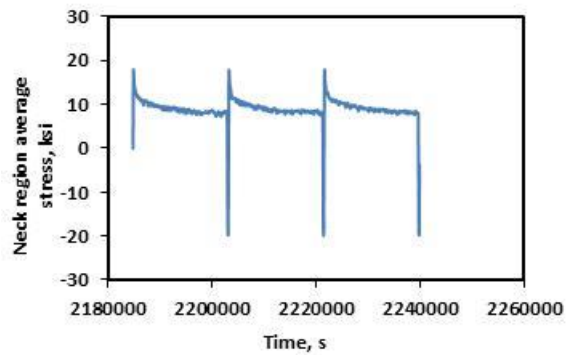
(a) Strain range



(b) Max/Min stresses



(c) Hysteresis Loop



(d) Stress history

Fig. 21. Test results for test #24 (SS304H-815 °C)

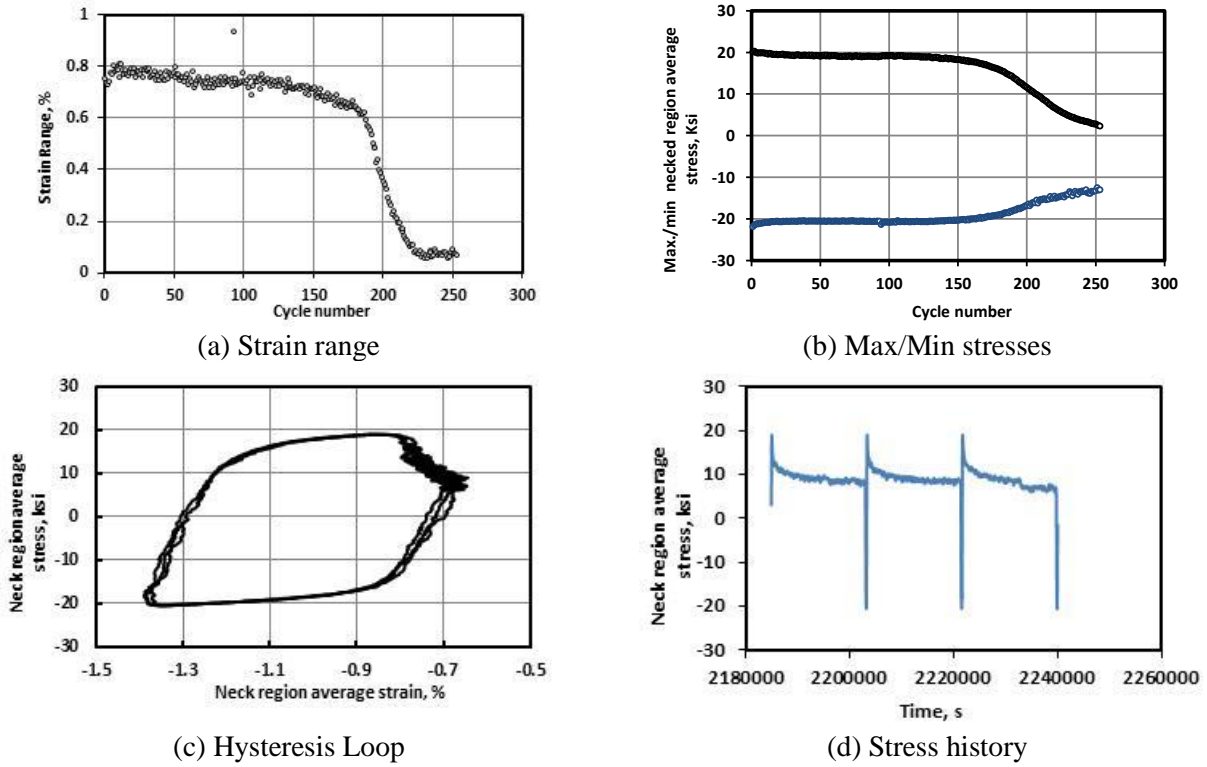


Fig. 22. Test results for test #25 (SS304H-815 °C)

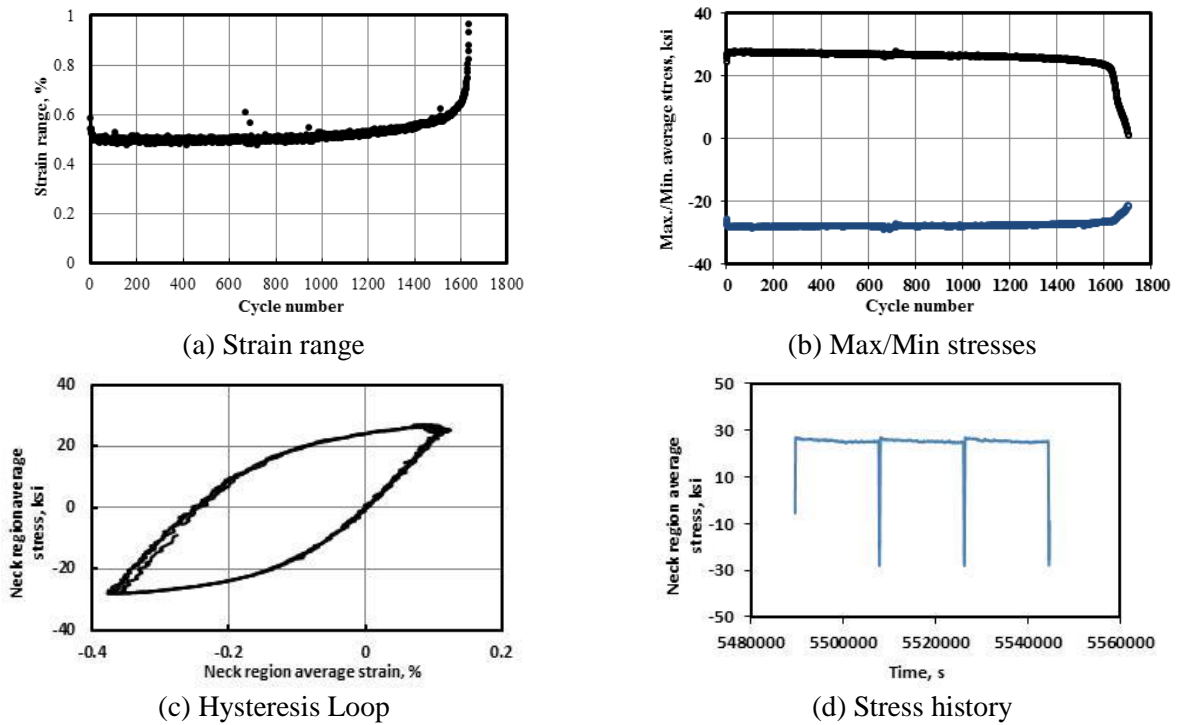


Fig. 23. Test results for test #26 (SS304H-650 °C)

Tests #24 and #25 at 815°C had similar responses as the initial strain range was similar, 0.60% and 0.78% respectively. As expected, Test #25 failed somewhat earlier due to the higher strain range. The hysteresis loops were relatively broad and there was significant stress relaxation during the hold period. Test #26 at a lower temperature, 650°C, and the same applied displacement amplitude as Test #25 lasted for almost a factor of ten more cycles. There was little stress relaxation but the hysteresis loops were relatively broad due to plasticity.

4.4 YSMT CREEP-FATIGUE TESTING OF SS316H

There was one YSMT test on SS316H at 815°C. This was a tubular specimen, sized to prevent buckling as described previously. The test parameters are shown in the following Table. Of particular note is the much higher follow-up factor, q . The capability to test specimens with high follow-up was the goal of the YSMT test setup.

Table 10. YSMT parameters

Necked test section extensometer gage length	Necked test section extensometer output for 10 volt	Driver section extensometer gage length	Drive section extensometer output for 10 volt	Represented driver section length	Resulted q value	Material Tested
0.5 in	30 mils	0.75 in	6 mils	2.7 in	6.5-7.0	SS316

A close-up photograph of the YSMT specimen of SS316H after testing is shown in Fig. 24 below. After testing, the necked test section showed significant barreling, the diameter at the center increased from 0.775in to 0.9in. There was virtually no diameter change at the failure location, the toe of the transition section.

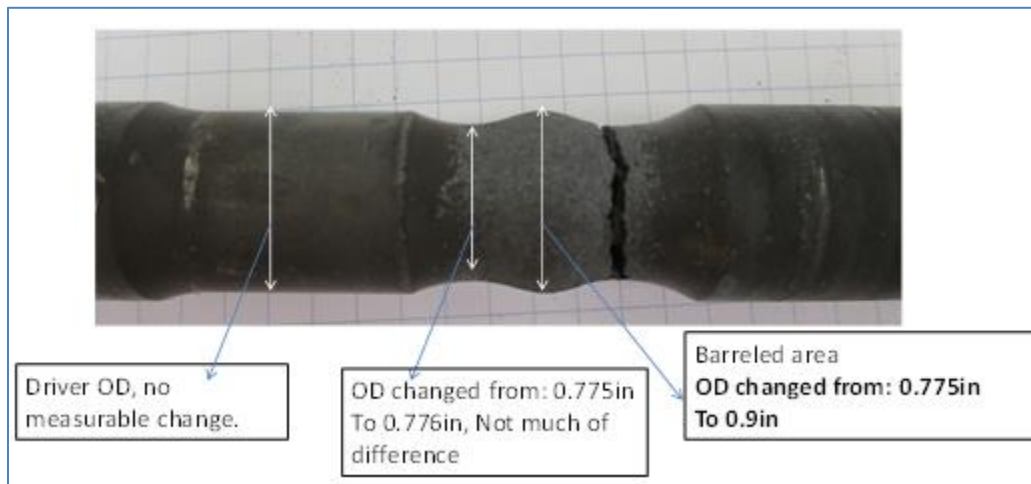


Fig. 24. Picture of YSMT specimen after testing

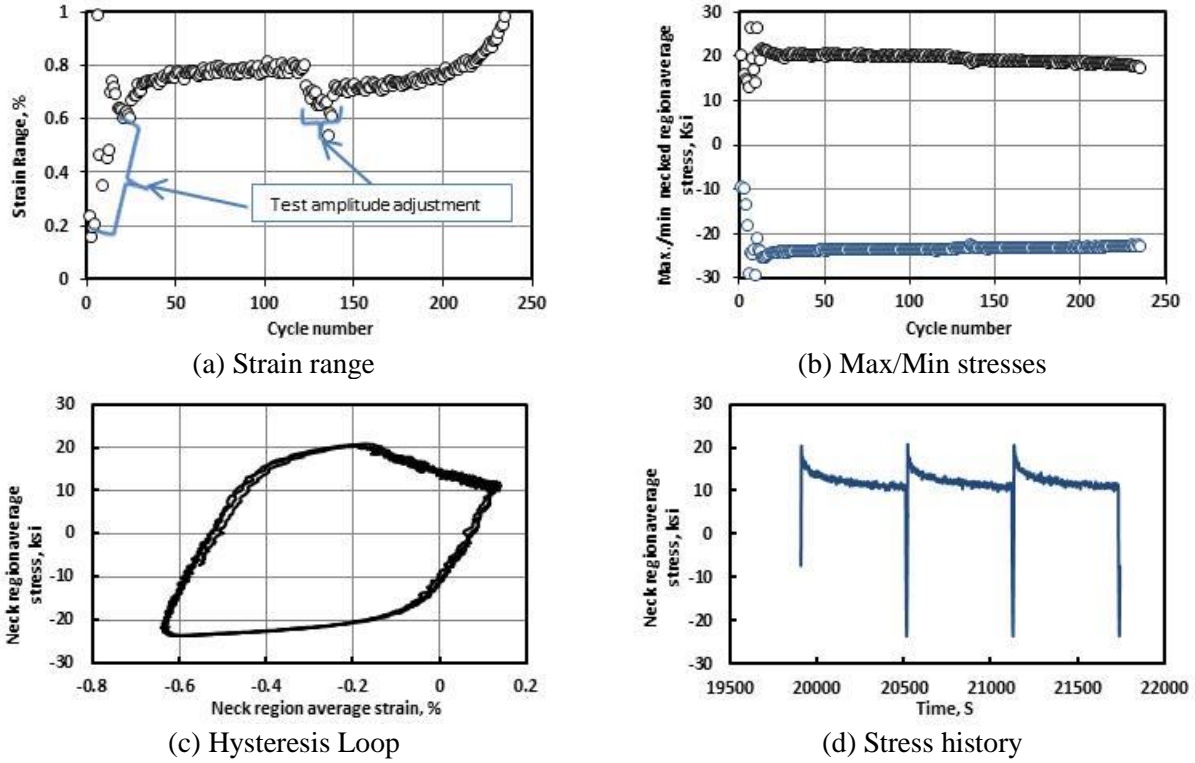


Fig. 25. Test results for YSMT tubular specimen(SS316-815 °C)

Fig. 25 shows plots of the measured strain range and maximum (tension) and minimum (compressive) stress as a function of cycle number, representative hysteresis loops and stress history for this YSMT test. It is interesting to compare the results of the YSMT test on SS316H to the results of Test #25 on SS304H, a similar material, both at 815°C. Both tests had an initial strain range of about 0.8% and stress of about 20ksi. The number of cycles to failure was about the same but the follow-up as observed from the hysteresis loops was much greater for the YSMT test.

5. CREEP-FATIGUE CODE CASE VERIFICATION

The Simplified Model Test (SMT) geometries, were developed to mock up the effects of elastic follow-up in reactor pressure boundary components. These data provide an opportunity to assess the conservatism of the E-PP creep-fatigue procedure developed for high temperature applications.

The proposed E-PP creep-fatigue code case specifies the use of a pseudo yield stress corresponding to a trial time T'_d that is greater than or equal to the design time t_{design} for the E-PP finite element analysis.

A trial time of $T'_d = t_{design}$ sets the critical condition for assessing if shakedown to elastic action would take place. That is, if an E-PP finite element analysis could not demonstrate shakedown to elastic action when $T'_d = t_{design}$ is used to set the pseudo yield stress, shakedown to elastic action would not take place for any other selected time $T'_d > t_{design}$ to set the pseudo yield stress.

5.1 TEST ARTICLE GEOMETRY AND TEST SETUP.

There were two SMT test article geometries used in the test program and they are shown in Fig. 26(a) and (b). They differ mainly in the root radius of the transition region.

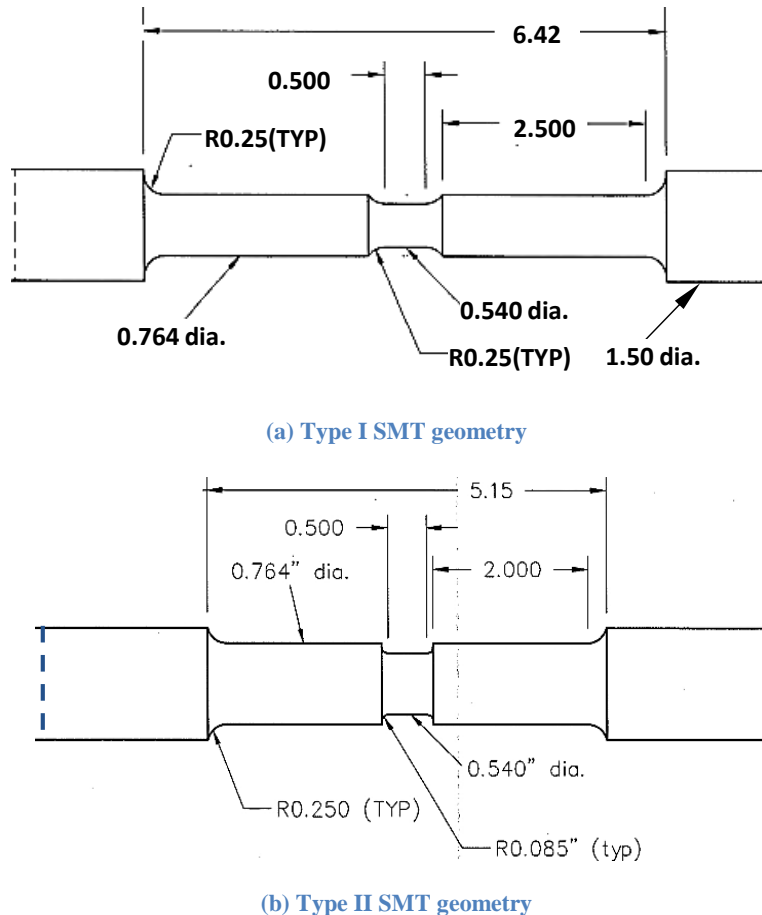


Fig. 26. Drawings for the Two SMT Test Articles (Dimensions in Inches)

Extensometer probes were mounted on the driver sections of the SMT test article over a gage length L , as shown in Fig. 27. The change in this gage length, ΔL , is controlled according to a prescribed cyclic profile. Another extensometer was mounted on the test section to measure the strain response independently.

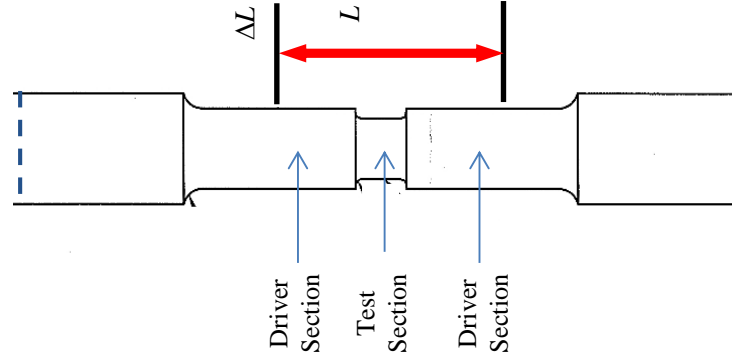


Fig. 27. Test setup of the SMT specimen.

5.2 ALLOY 617 SHAKEDOWN EVALUATION

5.2.1 Alloy 617 Material Parameters

The material parameters required in the E-PP creep-fatigue evaluation procedure are Young's modulus, E , shear modulus, G , yield strength, S_y , minimum rupture strength, S_r , and pseudo yield stress. The temperature dependence of E , G and S_y for Alloy 617 (from vendor data sheet), given in the units of MPa, are given as

$$E(T_k) = -7.57834280 \times 10^{-6} T_k^3 - 3.06384586 \times 10^{-3} T_k^2 - 52.8928996 T_k + 227.043102 \times 10^3 \quad (9)$$

$$G(T_k) = -6.14747367 \times 10^{-6} T_k^3 + 5.87486911 \times 10^{-3} T_k^2 - 25.2278723 T_k + 88.4508513 \times 10^3 \quad (10)$$

$$S_y(T_k) = 240 \times \left(\begin{array}{l} -2.78261712 \times 10^{-9} T_k^3 + 6.45428719 \times 10^{-6} T_k^2 \\ -4.96338300 \times 10^{-3} T_k + 1.98846231 \end{array} \right) \quad (11)$$

where T_k is the absolute temperature in kelvin. The data for S_y were based on testing to high temperature ASTM tensile testing standard.

The correlation for the minimum rupture strength in the units of MPa was given by Eno et al. (2008) as:

$$S_r = A^{-1/m} \exp\left(-\frac{Q}{mRT_k}\right) t_r^{1/m} \quad (12)$$

where t_r is the rupture time in hours and

$$A = \exp(\beta_0), \quad Q = R\beta_1, \quad m = \beta_2 + \beta_3 / T_k$$

$$\beta_0 = -[20.07 + 0.356z] \times \ln(10), \quad \beta_1 = 37531 \times \ln(10), \quad \beta_2 = 1.20, \quad \beta_3 = -7568 \quad (13)$$

$$z = 1.645, \quad R = 8.31447215$$

The pseudo yield stress, developed from tensile data from Huntington data package, is given as:

$$\text{pseudo yield stress} = \text{lesser of } (S_y, K'S_r) \quad (14)$$

where K' is a design factor that has a value of 0.9.

5.2.2 Alloy 617 Test Conditions Evaluation

There were seven SMT tests used for this evaluation, some of which were reported previously. The details of the test conditions are shown in Table 11. The cyclic profiles of ΔL prescribed for these tests are shown in Fig. 28. It is seen that fully reversed cycles, with tensile hold times at the ΔL peak, were imposed on the SMT test articles. It is also noted that the displacement rate for case (c) is approximately two orders of magnitude slower than the other cases.

Table 11. SMT test conditions and data for Alloy 617

Case	Spec. Geom. Type	Test Temp. (C)	Gage Length, L (mm)	ΔL Cyclic Profile (see Fig. 28)	Hold Time (s)	Time per Cycle (h)	Cycles to Failure	Life Time (h)
1	Type I	950	127.0	(a)	600	0.17	450	76.5
2	Type I	950	127.0	(b)	600	0.17	1000	170.0
3	Type I	950	127.0	(c)	600	0.50	950	475.0
4	Type I	950	127.0	(d)	180	0.05	1050	56.0
5	Type II	950	73.7	(e)	600	0.17	370	62.9
6	Type II	950	73.7	(e)	600	0.17	350	59.5
7	Type II	950	73.7	(f)	600	0.17	940	159.8

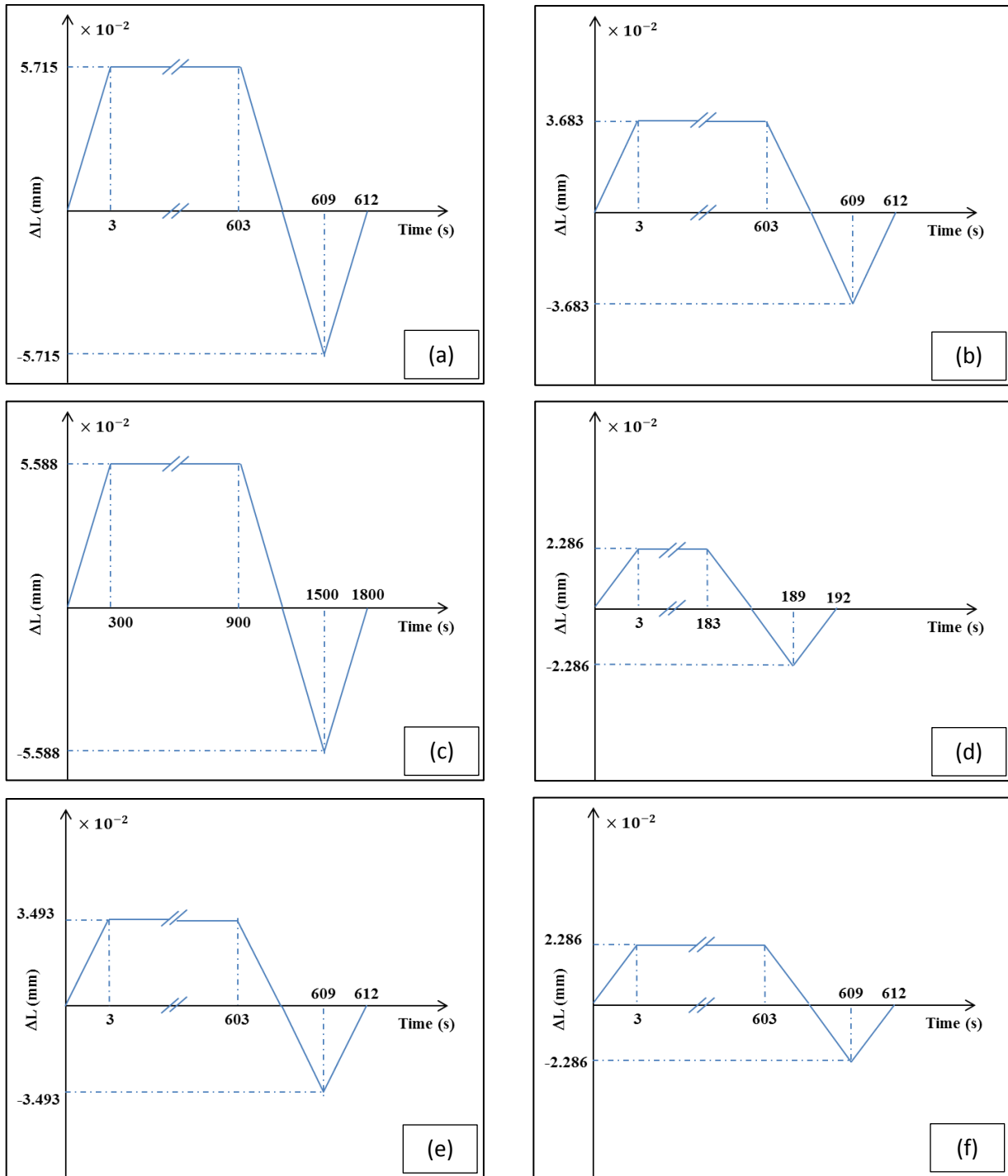


Fig. 28. Profiles of ΔL for imposing the prescribed displacements over the gage length L for Alloy 617. Displacement hold was applied at the maximum tensile ΔL value. Cycles were fully reversed.

For the consideration of these set of tests with respect to the E-PP creep-fatigue procedure, the design time is taken to be the life time of the creep-fatigue test specimen, and hence it is calculated as time per cycle multiplied by the observed/measured cycles to failure.

The first analysis step of the E-PP Creep-Fatigue Code Case is to seek an elastic shakedown response from the loading of a composite cycle using an appropriately chosen pseudo yield stress in an elastic-perfectly plastic model. Under this assumption, whether an elastically shakedown state can be achieved in an elastic-perfectly plastic model depends on the relative magnitude of the elastic stress range and “twice yield”, generally. There will be no elastic shakedown response if the elastic stress range, calculated as the product of the Young’s modulus and the total strain range, exceeds “twice yield”.

The use of the design time as the trial time for the determination of the pseudo yield stress will provide a critical condition for assessing if an elastic shakedown state can be achieved. Thus using such a choice for the trial times, the pseudo yield stresses were computed from Eqs. Eq. (11-14). E-PP finite element analyses were then performed for the seven cases listed in Table 11. Typical axisymmetric, quarter-symmetric finite element meshes for Types I and II SMT test articles are shown in Fig. 29. For each case, finite element analysis for 15 cycles was carried out.

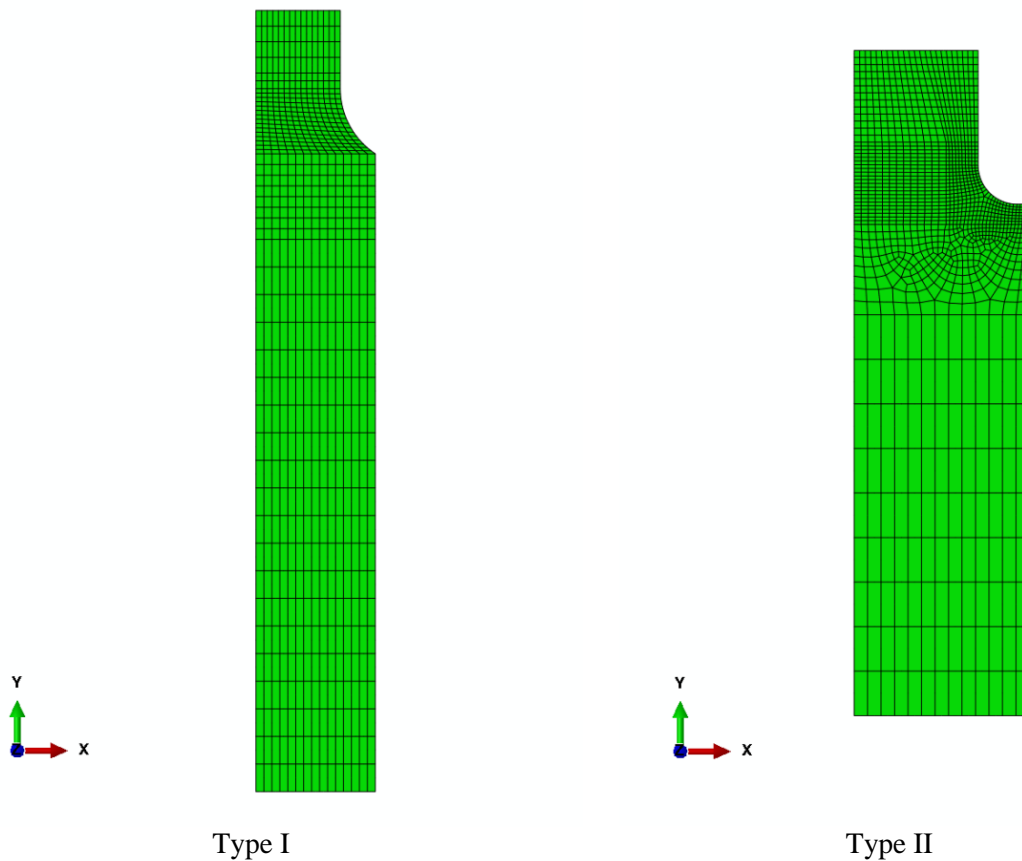


Fig. 29. Typical axisymmetric finite element meshes for Type I and Type II SMT test articles

In the first analysis step of the E-PP Creep-Fatigue Code Case, an elastic shakedown state is sought from the finite element results. Achieving an elastic shakedown state means that the incremental response for every integration point in the finite element mesh, and every time increment within a cycle, is elastic. Plasticity accumulated in previous cycles is permitted.

There are a number of ways to assess whether an elastic shakedown state is achieved for a cycle from the finite element results. General purpose finite element code ABAQUS was used for the finite element analyses in this study. In ABAQUS, a history variable called AC YIELD is provided for each integration point to store the information on whether an integration point has active plasticity for the current time

increment. Such a condition can be detected easily within ABAQUS internal plasticity routines. If plasticity is active for the current time increment, AC YIELD has a value of one, and if not, i.e., the incremental response is elastic, AC YIELD is zero. Post-processing scripts were developed to extract the information on AC YIELD for every integration point, every time increment, and every cycle. Using these results, elastic shakedown was not achieved for each of the seven SMT test cases. Some of the input material parameters for the E-PP finite element analyses are given in Table 12 for completeness. The E-PP Creep-Fatigue Code Case procedure (ASME C&S CONNECT Record Number 14-1446) would predict zero allowable creep-fatigue cycles for all these seven cases.

Table 12. Material parameters used in the E-PP finite element analyses for Alloy 617

<i>Case</i>	<i>E (MPa)</i>	<i>G (MPa)</i>	<i>Sy (MPa)</i>	<i>Sr @ Life Time (MPa)</i>	<i>PYS @ Life Time, K'=0.9 (MPa)</i>	<i>Elastic Shake-Down? (Y/N)</i>	<i>Allowable CF Cycles from E-PP-CF Code Case</i>
1	143910	55139	115.7	43.0	38.7	N	0
2	143910	55139	115.7	36.6	33.0	N	0
3	143910	55139	115.7	29.8	26.8	N	0
4	143910	55139	115.7	45.8	41.2	N	0
5	143910	55139	115.7	44.7	40.3	N	0
6	143910	55139	115.7	45.2	40.7	N	0
7	143910	55139	115.7	37.1	33.4	N	0

Application of the Code Case rules to these tests led to the predictions of zero allowable creep-fatigue cycles, and this simply means that designs under these temperatures and strain cycles are not viable.

5.3 SS316H SHAKEDOWN EVALUATION

The details of the SS316H SMT test conditions used in this evaluation are shown in Table 13. The cyclic profile of ΔL prescribed for the 316H test is shown in Fig. 30.

Table 13. SMT test conditions and data for 316H SS

<i>Spec. Geom. Type</i>	<i>Test Temp. (C)</i>	<i>Gage Length, L (mm)</i>	<i>Hold Time (s)</i>	<i>Time per Cycle (h)</i>	<i>Cycles to Failure</i>	<i>Life Time (h)</i>
Type I	815	127.0	600	0.17	400	68

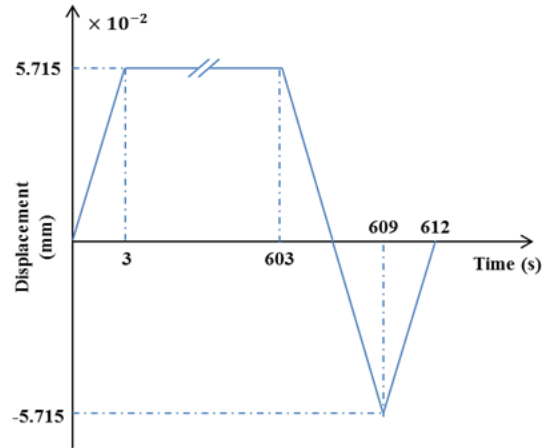


Fig. 30. Profile of ΔL for imposing the prescribed displacements over the gage length L for 316H.

E-PP finite element analysis was carried out for the conditions described in Table 13 and Fig. 30, using the finite element mesh for Type I geometry shown in Fig. 29. As noted above, the first step in the E-PP Creep-Fatigue Code Case is to seek an elastic shakedown state from the finite element result. The input material parameters for the E-PP finite element analysis are given in Table 14. The E-PP Creep-Fatigue Code Case procedure also predicts zero allowable creep-fatigue cycles for the 316H case.

Table 14. Material parameters used in the E-PP finite element analysis for 316H

E (MPa)	G (MPa)	S_y (MPa)	S_r @ Life Time (MPa)	PYS @ Life Time, $K'=0.9$ (MPa)	Elastic Shake-Down? (Y/N)	Allowable CF Cycles from E-PP-CF Code Case
127193	48920	75.15	54.08	48.68	N	0

5.4 COMPARISON BASED ON ALLOWABLE DESIGN LIFE

In the preceding comparisons, the pseudo yield strength was limited by the tabulated yield strength. The relatively low value of pseudo yield strength prevented elastic shakedown for the high load levels required to achieve relatively short test durations. In a typical component design, the design life would be about three orders of magnitude longer than the test duration and the pseudo yield stress would typically be limited by the creep-rupture strength. Failure to achieve elastic shakedown is a “go, no-go” type criteria and doesn’t provide a quantitative assessment of the design margin. To get such a quantitative assessment it is necessary to disregard the yield strength and use an extrapolation of the creep-rupture strength to an allowable design life that is shorter, perhaps significantly shorter, than the test duration. As the life is shortened the extrapolated creep rupture stress, and hence the pseudo yield strength, becomes higher. Then, comparing the allowable design life to the measured test life provides a quantitative design margin assessment.

To implement this procedure, three Alloy 617 test cases were selected with varying loading amplitudes as shown in Table 15. Using the ABAQAS finite element model the required pseudo yield stress for elastic shakedown was determined. From that value, the required time to rupture was determined by taking into account the design factor K' . From the time to rupture and cycle frequency, the

allowed number of cycles was determined. The applicable strain range was determined in accordance with the code case and the fatigue damage fraction determined from the allowable number of cycles. The allowable creep damage was then determined from the damage diagram (0.1, 0.1 intercept) for the calculated fatigue damage. The allowable time was then determined by multiplying the previously determined required time to rupture by the allowable creep damage fraction. The resulting Alloy 617 design margins are illustrated in Fig. 31.

Table 15. Experimental Data – Alloy 617 at 950°C

<i>Test Num.</i>	<i>Amplitude (mils)</i>	<i>Holding time (s)</i>	<i>Loading time (s)</i>	<i>Cycle number to failure</i>	<i>Allowed lifetime (hrs)</i>
1	1.8	180	3	1050	56
2	2.9	600	3	1000	170
3	4.5	600	3	450	77

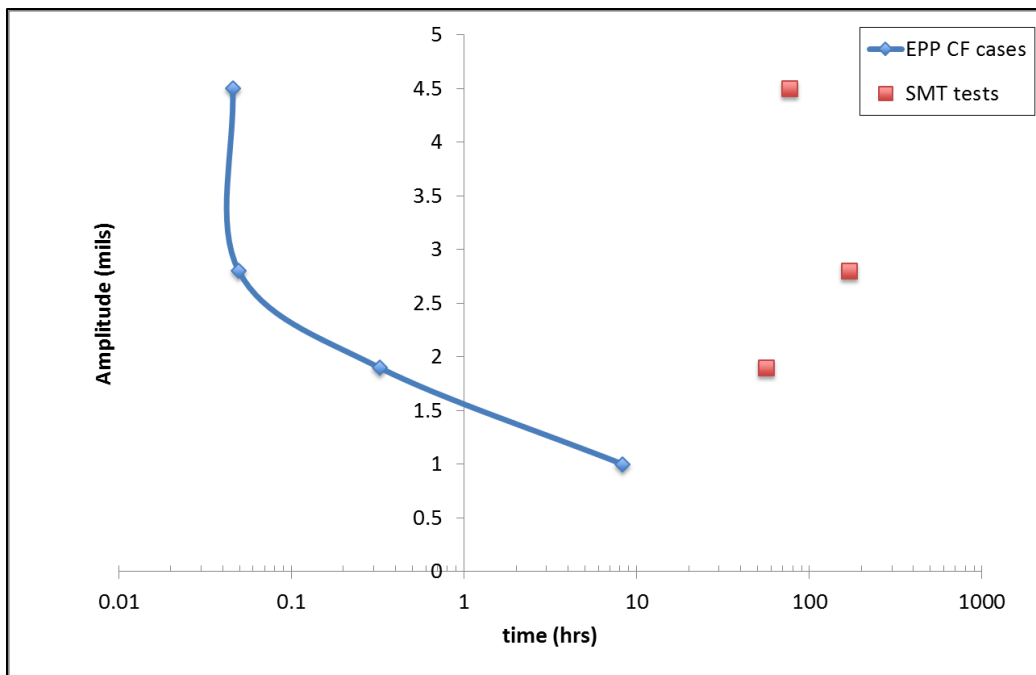


Fig. 31. Creep-fatigue code case allowable life comparison to Alloy 617 SMT data

As shown in Table 16 and Fig. 32, a similar comparison was done for 316H stainless steel tested at 815°C.

Table 16. Experimental Data – SS316H at 815°C

Test Num.	Amplitude (mils)	Holding time (s)	Loading time (s)	Cycle number to failure	Allowed lifetime (hrs)
1	1.9	600	3	410	69.7
2	4.5	600	3	13,214	1226

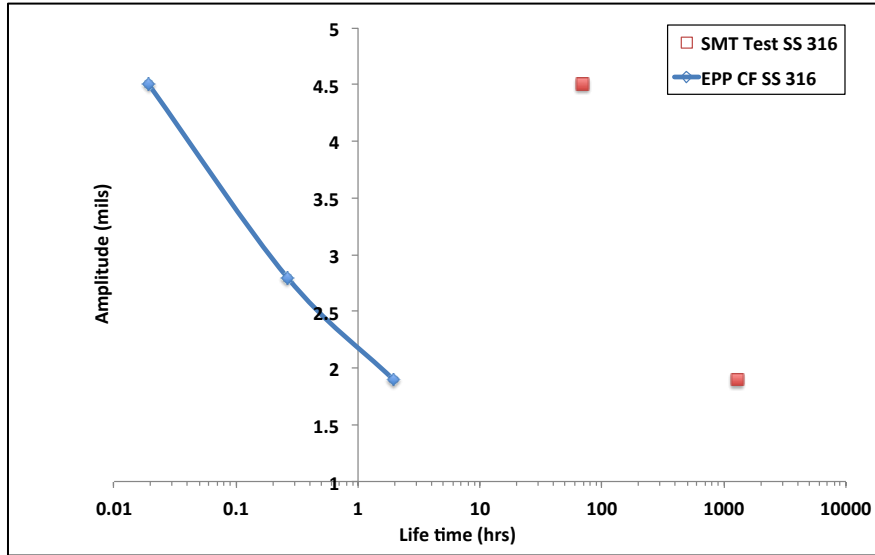


Fig. 32. Creep-fatigue code case allowable life comparison to SS316H SMT data

From Fig. 31 and Fig. 32 it is evident that there is a significant design margin between the Creep-fatigue Code Case allowable life and the experimentally measured life for both Alloy 617 and 316H stainless steel.

6. SUMMARY

The current rules in Subsection NH for evaluation of creep-fatigue damage are based on the separation of the combined effects into creep damage and fatigue damage. The creep damage is evaluated by dividing the time at a particular stress level by the allowable time to rupture at that stress level. This is a linear time fraction damage summation. The fatigue damage is calculated by dividing the number of cycles at a particular strain range by the number of cycles at that strain range as determined from continuous cycling fatigue tests (Miner’s Rule). The interaction due to the combined effects of creep and fatigue are addressed through an allowable damage interaction, or D diagram. The SMT methodology is based on test data generated from specimens sized to represent and bound the response of real structures and loading conditions. This methodology does not require a D diagram and does not utilize the linear time fraction summation of creep damage.

The data generated to support the development of the SMT design curves also support the verification of proposed advanced design methods based on elastic-perfectly plastic (E-PP) analysis. These data also

support the development and verification of constitutive equations for inelastic analysis. Both the E-PP design methods and the SMT approach to creep-fatigue evaluation address the restriction on the use of current Subsection NH simplified evaluation methods for Alloy 617 above $650^{\circ}C$ ($1200^{\circ}F$).

The feasibility of the SMT methodology and a new testing method, YSMT, have been demonstrated through the development of test frames and supporting hardware, instrumentation and measurement technology and specimen development. A tubular specimen was developed for YSMT testing to avoid the bucking issue experienced with solid bar specimens tested to high follow-up values.

Results from the SMT tests on both Alloy 617 and SS316H were compared to the predictions from the EPP Creep-Fatigue Code Case. Two different comparisons were made; one based on design life equal to the test duration and the other with an acceptable design life determined from the EPP Code Case procedure. The latter approach permits the determination of a quantitative margin while the former is a “go-no go” comparison. In all cases it is evident that there is a significant design margin between the Creep-fatigue Code Case allowable life and the experimentally measured life for both Alloy 617 and 316H stainless steel.

7. REFERENCES

- ASTM E2714 – 09, (2009), “Standard Test Method for Creep-Fatigue Testing”, ASTM International, West Conshohocken, PA, DOI:10.1520/E2714–09E01, www.astm.org.
- ASTM E83 – 10a, (2009), “Standard Practice for Verification and Classification of Extensometer Systems”, ASTM International, West Conshohocken, PA, DOI:10.1520/E00834–10A, www.astm.org.
- ASME Boiler and Pressure Vessel Code, (2013), “Rules for construction of Nuclear Facility Components”, Division 1-subsection NB Class 1 Components, 2013, American Society of Mechanical Engineers, New York, NY.
- ASME C&S CONNECT Record Number 14-1446.
- Broyles, R. K., (1995), “Bellows High Temperature Cycle Life,” PVP-Vol. III, No. 3, American Society of Mechanical Engineers Press, New York, New York.
- Carroll, L., (2012), “Creep-Fatigue of Alloy 617,” presented at VHTR R&D FY12 Technical Review Meeting, May 22-24, 2012, Salt Lake City, Utah.
- Carroll, M. C. and Carroll, L. J., (2013), “Developing Dislocation Subgrain Structures and Cyclic Softening During High-Temperature Creep–Fatigue of a Nickel Alloy” *Metallurgical and Materials Transactions A*, 44A, pp. 3592-3607.
- Carroll L.J., Cabet, C., Carroll, M. C., Wright, R. N., (2013), “The development of microstructural damage during high temperature creep–fatigue of a nickel alloy” *International Journal of Fatigue*, 47, pp.115-125.
- Corum, J. M., and Blass, J. J., (1991), Rules for Design of Alloy 617 Nuclear Components to Very High Temperatures, ASME PVP Vol. 215, pp.147-153.
- Eno, R., G.A. Young, and T.-L. Sham, (2008), “A Unified View of Engineering Creep Parameters,” Proceedings of the ASME 2008 Pressure Vessels and Piping Division Conference, Chicago, Illinois, July 2008, Paper No. PVP2008-61129, American Society of Mechanical Engineers, New York, NY.
- INCONEL 617 Datasheet, <http://www.specialmetals.com/documents/Inconel%20alloy%20617.pdf>.
- Jawad, M.H. and Jetter, R. I. (2009) *Design and Analysis of ASME Boiler and Pressure Vessel Components in the Creep Range*, American Society of Mechanical Engineers Press, New York, New York.
- Jetter, R. I., (1998), “An Alternate Approach to Evaluation of Creep-Fatigue Damage for High Temperature Structural Design Criteria,” PVP-Vol. 5 Fatigue, Fracture and High Temperature Design Methods in Pressure Vessel and Piping, Book No. H01146 – 1998, American Society of Mechanical Engineers Press, New York, New York.
- Kasahara, N., Nagata, T., Iwata, K. and Negishi, H., (1995), “Advanced Creep-Fatigue Evaluation Rule for Fast Breeder Reactor Components: Generalization of Elastic Follow-up Model,” *Nuclear Engineering and Design*, Vol. 155, pp. 499-518.
- Takahara, K., Ueta, M., Dousaki, K. Wada, H., Hayashi, M., Ozaki, H., and Ooka, Y., (1995), "Elevated Temperature Structural Design Guide for DFBR in Japan," *Transactions of the 13th International Conference on Structural Mechanics in Reactor Technology*, Vol. 1, P380.
- T.-L. Sham, Yanli Wang, Robert I. Jetter and Hongyu Zhou, (2012), “Report on Progress in Development of Creep-Fatigue Design Method and Experimental Parameters Based on Simplified Model Test Approach” ORNL/TM-2012/428, September 20, 2012.
- Yanli Wang, Robert I. Jetter and T.-L. Sham, (2013), “Application of Combined Sustained and Cyclic Loading Test Results to Alloy 617 Elevated Temperature Design Criteria”, ORNL/TM-2014/294, August 25, 2014.
- Yanli Wang, Robert I. Jetter and T.-L. Sham, (2013), “Report on Alloy 617 SMT Creep-Fatigue Scoping Test”, ORNL/LTR-2013/600, December 16, 2013.

ELECTRONIC DISTRIBUTION

Name	Affiliation	Email
Baird, S.T.	ORNL	bairdst@ornl.gov
Carroll, L.	INL	Laura.Carroll@INL.gov
Corwin, W.	DOE	william.corwin@nuclear.energy.gov
Hill, R.N.	ANL	bobhill@anl.gov
Jetter, R.I.	Consultant	bjetter@sbcglobal.net
Lara-Curzio, E.	ORNL	laracurzioe@ornl.gov
Li, M.	ANL	mli@anl.gov
Petti, D.	INL	David.Petti@inl.gov
Pu, C.	University of Tennessee	cpu@utk.edu
Sham, T.-L.	ORNL	shamt@ornl.gov
Sink, C.	DOE	carl.sink@nuclear.energy.gov
Wang, H.	ORNL	wangh@ornl.gov
Wang, Y.	ORNL	wangy3@ornl.gov
Wright, R.N.	INL	richard.wright@inl.gov

ORNL Office of Technical
Information and Classification